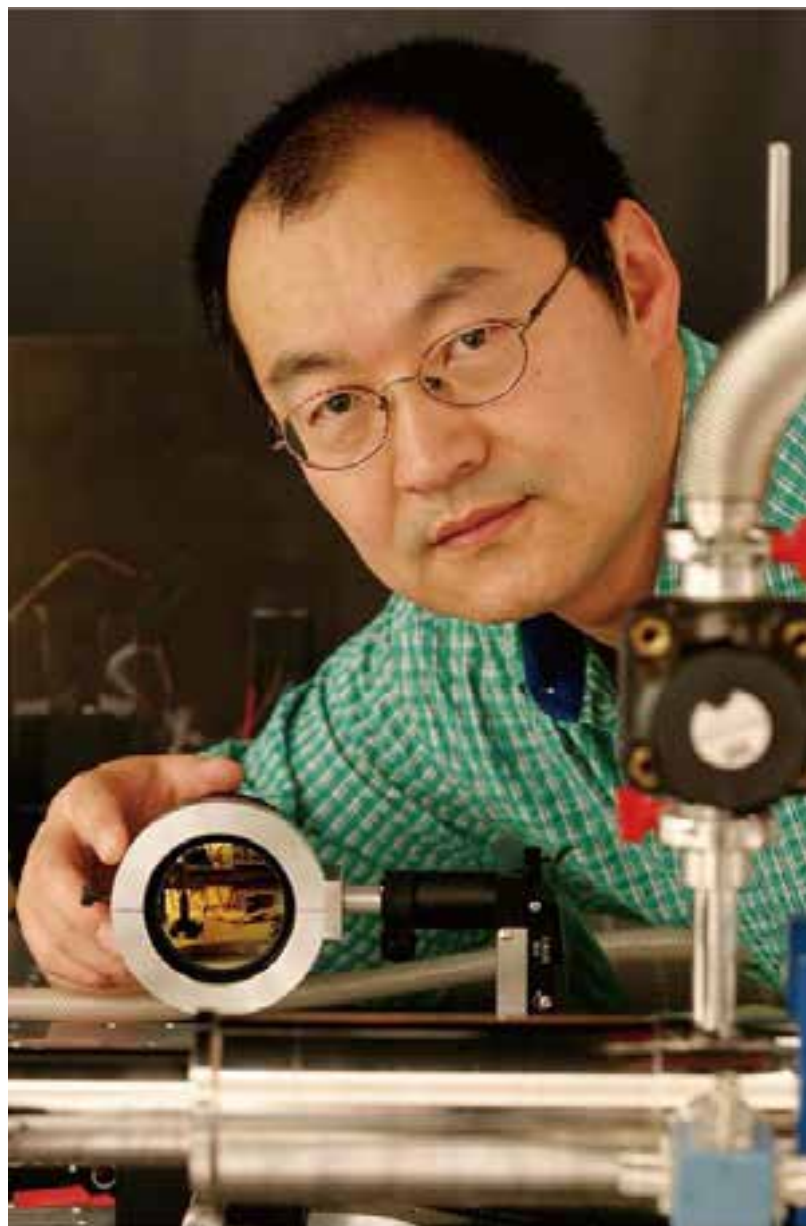


In memory of H. C. Liu (1960.3.26 – 2013.10.23)



H. C. received his undergraduate education from Lanzhou University, China, in Class 1978



H. C. went to Univ. Pittsburg in 1982, as a member of the 1982 class of CUSPEA program.

From Wikipedia, the free encyclopedia

CUSPEA (China-U.S. Physics Examination and Application) was an examination and admission system used by the physics departments of some American and Canadian universities for graduate school admission from People's Republic of China between 1979 and 1989.

It was created by the Chinese-American physicist **Tsung-Dao Lee** and Chinese physics community as an alternative graduate school admission procedure. At that time in China, higher education was still recovering from the Cultural Revolution; school transcripts and recommendation letters were difficult to evaluate. Furthermore, standardized tests such as the Graduate Record Examination were unavailable in China.

H. C. is a pioneer in intersubband devices and physics, organized the 2nd ITQW Conference in 1993

9th International Conference on Intersubband Transitions in Quantum Wells

ITQW`07 will be the key event in 2007 in the area of intersubband transitions in quantum wells and intersublevel transitions in quantum dots. It is aimed at bringing together researchers from academia, government and industrial laboratories for scientific interaction, the showcasing of new results in the fields and debate on future trends. The conference series has a history dating back to 1991 with the first meeting in Cargese, France, followed by meetings in **Whistler, Canada (1993)**, Ginosar, Israel (1995), Tainan, Taiwan (1997), Bad Ischl, Austria (1999), Monterey, USA (2001), Evolene, Switzerland (2003) and Cape Cod, USA (2005).

H. C.'s early contribution to QCL

*K. M. Bulak, S. B. Phatak, and J. P. Shaver, IEEE Trans. Electron Devices ED-37, 422 (1990).
 *K. Mats, M. Kinagaki, S. Nakatsuka, and K. Takahashi, Jpn. J. Appl. Phys. Suppl. 21-2, 99 (1992).
 *C. Amann, A. Shikharova, and M. Yamaguchi, J. Appl. Phys. 84, 3780 (1998).
 *C. R. Lewis, C. W. Ford, G. F. Vintup, B. A. Aron, R. T. Green, and J. G. Wuerhan, in Proceedings of the 1984 Photonic Specialist Conference, Las Vegas, 1985 (IEEE, New York, 1985), p. 356.
 *K. A. Prior, G. J. Davies, and R. Hockingstone, J. Cryst. Growth 64, 55 (1984).
 *C. van Opdyck, R. C. Fries, and M. Klari, Appl. Phys. Lett. 24, 23 (1974).

*T. Junturi, J. Lagowski, and H. C. Gatos, Appl. Phys. Lett. 25, 537 (1975).
 *P. D. Kirchmer, J. M. Woodhill, J. L. Freund, and G. D. Petro, Appl. Phys. Lett. 38, 427 (1981).
 *J. Lagowski, D. G. Liu, T. Aoyama, and H. C. Gatos, Appl. Phys. Lett. 44, 536 (1984).
 *K. Akimoto, M. Kamada, K. Taira, and N. Watanabe, J. Appl. Phys. 69, 2439 (1990).
 *C. Amann, M. Yamaguchi, and A. Shikharova, in Technical Digest on the International Photonic Science and Engineering Conference, Kyoto, Japan, 1984 (Japan Society of Applied Physics, Tokyo, 1984), p. 345.

A novel superlattice infrared source

H. C. Liu

Microstructural Sciences Laboratory, National Research Council, Ottawa K1A 0R6, Canada

(Received 6 October 1987; accepted for publication 4 December 1987)

A novel superlattice infrared source is proposed. The device utilizes radiative intersubband transitions and resonant tunneling phenomena in a finite superlattice. Theoretical estimates of the radiative transition lifetime and resonant tunneling time are given, which show the possibility of obtaining an infrared light-emitting diode, or even a laser. The device has a narrow emission spectrum, and the wavelength can be adjusted by varying device parameters. The device design has no long wavelength limitation. A specific design of an AlGaAs-GaAs 10- μm superlattice infrared source is discussed.

Recently, several research groups have reported studies on intersubband transitions in superlattices and quantum wells. Applications ranging from digital logic devices¹ and light modulators² to infrared (IR) detectors^{3,4} have been considered. Theoretical studies of the physical process and device applications have been undertaken.⁵⁻⁷ All of the above studies involve photoexcitations of electrons from a lower subband to a higher subband. In this communication, we consider the reverse process, i.e., the photoemission process between subbands in a superlattice or a quantum well. The obvious application of the photoemission process is an IR source, i.e., an IR light-emitting diode or a laser.

Kazarinov and Suris⁸ examined the possibility of the amplification of electromagnetic waves in a semiconductor superlattice. Capasso and co-workers⁹ investigated sequential resonant tunneling, but the emission effect has not yet been observed experimentally. Here, we propose a special superlattice structure which gives several improvement factors to make the photoemission process favorable. The device structure is shown in Fig. 1, which is a finite superlattice consisting of alternating narrow and wide wells separated by barriers. The AlGaAs-GaAs material system can be used. The narrow well is designed to have only one quasibound state E_1^* , while the wide well has two states (E_0 and E_1). Under zero bias (upper part in Fig. 1), we have $E_1^* = (E_0 + E_1)/2$ by adjusting the well widths, w' and w . When biased to the operating point (lower part in Fig. 1), electrons are injected into the higher state of the wide well (E_1) via resonant tunneling through E_1^* , and hence, the in-

jection process is efficient (i.e., the tunneling probability is close to one). An electron in the higher state (E_1) can emit a photon ($h\nu$), and relax to the lower state (E_0). The relaxed electron continues to tunnel resonantly to the next wide well, and emits another photon, and so on. The process described above could result in an amplification of the IR radiation, and hence, an IR emitting device. The barrier widths are adjusted to be thin enough so that the tunneling time through a double-barrier structure between two adjacent wide wells is somewhat faster than the radiative relaxation time. Compared with the simple superlattice structures,^{8,9} the present device offers efficient and rapid electron transfers between active regions (i.e., wide wells) and hence, favors the radiative emission processes. This scheme also offers the possibility of obtaining a population inversion between the higher and the lower states.

Experimentally, an excited state lifetime of about 0.1 ps was reported for AlGaAs-GaAs quantum wells with a two-dimensional electron gas in the ground state subband and for about 10- μm separation between the ground state and the first excited state subbands.^{10,11} If we assume that the 0.1-ps lifetime is due to nonradiative processes, e.g., phonon scatterings and electron-electron scatterings, we then need to have a radiative relaxation time faster than about 0.1 ps. We give a theoretical estimate of the radiative lifetime below. For simplification, we consider a single quantum well with one electron in the first excited state ($|1\rangle$) and no electrons in the ground state ($|0\rangle$) initially. A photon field (propagating laterally) polarized in the growth direction (z) can be

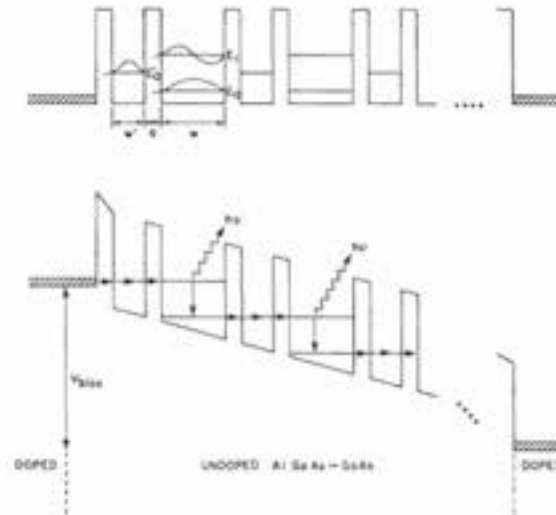


FIG. 1. Upper part: conduction-band edge profile of the proposed device under no bias. Lower part: biased device in operation. Heavily doped contact layers at either ends of the structure are included to show the Fermi level. Photon ($h\nu$) emission processes occur in the wide wells.

described by the following vector potential (operator):

$$\mathbf{A} = \sum_{\mathbf{q}} \left(\frac{\hbar}{2\epsilon V \omega_{\mathbf{q}}} \right)^{1/2} \left[a_{\mathbf{q}} e^{-i\mathbf{q}\cdot\mathbf{r}} e^{-i\omega_{\mathbf{q}}t} + a_{\mathbf{q}}^\dagger e^{i\mathbf{q}\cdot\mathbf{r}} e^{i\omega_{\mathbf{q}}t} \right], \quad (1)$$

where ϵ is the material dielectric constant multiplied by the free space permittivity, V is the normalization volume, $\omega_{\mathbf{q}}$ is the angular frequency of a photon with wave vector \mathbf{q} , \mathbf{q} is in the x - y plane, $\hat{\mathbf{z}}$ is the photon polarization vector, i.e., a unit vector in z direction, and $a_{\mathbf{q}}^\dagger$ ($a_{\mathbf{q}}$) is the creation (annihilation) operator for the mode \mathbf{q} photon. Using a dipole interaction $H_{int} = -e\mathbf{A}\mathbf{q}/m$, the matrix element is found to be

$$\langle 1|H_{int}|0\rangle = -\frac{e}{m} \left(\frac{\hbar}{2\epsilon V \omega_{\mathbf{q}}} \right)^{1/2} \langle 1|p_z|0\rangle \sqrt{n_{\mathbf{q}}+1}, \quad (2)$$

where $n_{\mathbf{q}}$ is the number of \mathbf{q} -mode photons and $\mathbf{q} = \mathbf{k}_i - \mathbf{k}_f$ with \mathbf{k}_i (\mathbf{k}_f) being the initial (final) two-dimensional electron wave vector. Employing Fermi's golden rule, the transition rate (Γ) is

$$\Gamma = \frac{2\pi}{\hbar} \sum_{\mathbf{q}} |\langle 1|H_{int}|0\rangle|^2 \delta(E_1 - E_0 + \hbar\omega_{\mathbf{q}}) = \frac{e^2}{4\epsilon L \hbar} f(n_{\mathbf{q}}+1), \quad (3)$$

where the oscillator strength $f = (2m/\hbar^2) |\langle 1|p_z|0\rangle|^2 / E_1(E_1)$, $E_1(E_0)$ is the initial (final) total electron energy, L is the thickness in which the photon field is confined, and L could be the distance between two heavily doped contact layers and also in the structure shown in Fig. 1, L is equivalent to the thickness of one period of the superlattice. For the superlattice structure shown in Fig. 1, the total transition rate is

obtained by summing over all active wells [i.e., Eq. (3) is multiplied by the number of the superlattice periods]. On the other hand, the confinement length is the superlattice period multiplied by the number of periods, and hence, the number of periods cancels out, and we can take L to be the period in Eq. (3) to obtain the total transition rate. Because of the fact that the two contact layers on the top and the bottom of the superlattice are heavily doped (conducting), photon fields are confined in the undoped superlattice structure. The oscillator strength (f) has a numerical value of roughly one.¹² For a thickness $L = 150$ Å, the spontaneous ($n_{\mathbf{q}} = 0$) radiative relaxation time ($1/\Gamma$) is about 0.05 ps which is smaller than 0.1 ps. The above discussion shows that it is possible to have the radiative transition to be the dominant relaxation process. Notice that we have assumed a zero electron population in the ground state. If there exists a two-dimensional electron sea in the ground state subband, the radiative transition rate is greatly reduced. To estimate the electron population in the ground state subband (n_0) relative to the first excited state subband (n_1), a simple rate equation is used:

$$\frac{dn_0}{dt} = \frac{n_1}{\tau_{tunnel}} - \frac{n_0}{\tau_{escape}}, \quad (4)$$

where τ_{tunnel} is the relaxation time ($1/\Gamma$) from E_1 to E_0 subbands, and τ_{escape} is the escaping time of an electron out of E_0 , which equals the tunneling time from E_0 to E_1 of the next wide well. In the steady state ($dn_0/dt = 0$), we get

$$n_0 = (\tau_{tunnel}/\tau_{escape}) n_1. \quad (5)$$

Optically pumped intersubband Raman laser

VOLUME 90, NUMBER 7

PHYSICAL REVIEW LETTERS

week ending
21 FEBRUARY 2003

Coupled Electron-Phonon Modes in Optically Pumped Resonant Intersubband Lasers

H. C. Liu,* C. Y. Song, Z. R. Wasilewski, and A. J. SpringThorpe

Institute for Microstructural Sciences, National Research Council, Ottawa, Canada K1A 0R6

J. C. Cao

Shanghai Institute of Microsystem and Information Technology, Chinese Academy of Sciences, Shanghai 200050, China

C. Dharma-wardana, G. C. Aers, D. J. Lockwood, and J. A. Gupta

Institute for Microstructural Sciences, National Research Council, Ottawa, Canada K1A 0R6

(Received 4 July 2002; published 20 February 2003)

Intersubband lasing at 12–16 μm based on a CO_2 laser pumped stimulated resonant Raman process in GaAs/AlGaAs three-level double-quantum-well structures is reported. The presence, or lack of, lasing action provides evidence for resonantly coupled modes of collective electronic intersubband transitions and longitudinal optical phonons. An anticrossing behavior of these modes is clearly seen when the difference between the pump and lasing energies (i.e., Stokes Raman shift) is compared with the subband separation. This work reveals the significance of the strong coupling between intersubband transitions and phonons and raises a new possibility of realizing a phonon “laser.”

DOI: 10.1103/PhysRevLett.90.077402

PACS numbers: 78.67.De, 42.55.Yc, 42.65.Dr, 78.45.+h

New physical phenomena and devices in the infrared and terahertz frequency regions have attracted much interest in recent years. The quantum-cascade laser (QCL) [1] is probably the most prominent and exciting example of new semiconductor devices both in terms of basic physics [2,3] and potential applications [4,5]. Being a unipolar device involving only electrons, the QCL operates by cascading many active stages. In contrast to the QCL, which is electrically pumped, optically pumped intersubband lasing has received only limited attention so far [6–9]. Optical pumping offers the advantage of highly selective excitation of carriers into the desired subband and thus provides a tool for the study of the lasing mechanism, carrier relaxation, and other processes.

In this Letter we report on experimental results from a systematic study of optically pumped infrared lasers based on the resonant intersubband Raman process. The Raman effect is widely used as an optical characterization tool in the study of semiconductors. Most experiments, though, are carried out in the near-infrared to visible spectral region, and very limited experiments were reported so far in the midinfrared [10,11]. The most important feature of the present work is the evidence of resonantly coupled modes comprising collective intersubband transitions (IT) and longitudinal optical (LO) phonons. Coupled modes in semiconductors were reported in the classic paper of Mooradian and McWhorter [12] on Raman scattering in doped bulk GaAs, which provided definitive evidence of coupled electron plasmon-phonon modes. Coupled electronic excitation-phonon modes have also been observed in other solid state systems [13]. Light scattering experiments have been used for the study of GaAs/AlGaAs heterostructures since the early days of the research in this field [14,15].

Our artificial three-level system is realized in a GaAs/AlGaAs asymmetric double quantum well (DQW). The use of the asymmetric DQW provides the flexibility in designing the desired level separations and affords strong dipole-matrix elements among all states. The structure and the Raman lasing characteristics are illustrated in Fig. 1. The Raman laser works by optical pumping from subband E_1 to E_3 and emitting from E_3 to E_2 . In the original (uncoupled intersubband-phonon) picture [9], the separation between E_1 and E_2 is made in near resonance with a given LO-phonon mode having a fixed phonon energy. All transitions are real (as opposed to virtual) and resonant with intersubband separations. If ω_{pump} , ω_{laser} , and ω_{phonon} are the pump, laser, and LO phonon frequencies, respectively, we then have $\omega_{\text{pump}} = \omega_{\text{laser}} + \omega_{\text{phonon}}$ for the Raman process. If the pump frequency is varied (within the 1-to-3 absorption linewidth), the lasing frequency must follow by exactly the same amount since the phonon frequency is fixed; i.e., $\omega_{\text{pump}} - \omega_{\text{laser}} = \omega_{\text{phonon}} = \text{const}$ for a given LO-phonon mode (see the bottom part of Fig. 1).

To obtain a sufficient gain and output power the DQW is repeated 150 times, separated by wide (20 nm) barriers, center-delta doped with Si to $3 \times 10^{11} \text{ cm}^{-2}$ with an uncertainty of $\pm 10\%$. The aluminum fraction in all AlGaAs barriers is fixed to 35% for all samples. A range of well thicknesses were used: 7.4–8.0 nm for the wide well and 4.7–6.1 nm for the narrow well, with the thin tunnel barrier fixed at 1.13 nm. The modulation doping in the wide barriers results in an electron population of $3 \times 10^{11} \text{ cm}^{-2}$ in each DQW. The active region is clad by appropriate waveguiding layers [7,8]. The experimental details (see also Ref. [8]) are as follows. The side-pumping cleaved-facet geometry was used. The excitation

VOLUME 90, NUMBER 7

PHYSICAL REVIEW LETTERS

week ending
21 FEBRUARY 2003

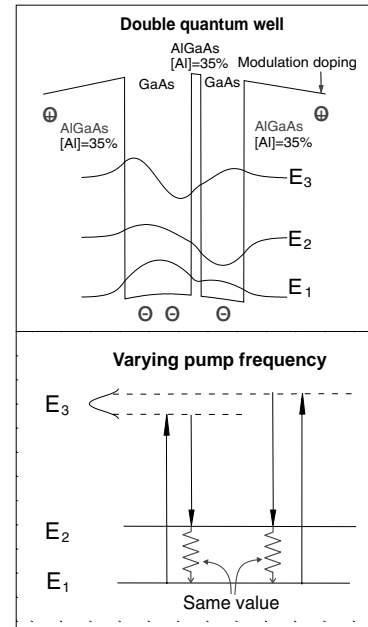


FIG. 1. Top: the calculated double quantum-well potential and wave functions; bottom: an illustration of the Raman lasing characteristics. When the pump frequency is varied within the linewidth of the 1-to-3 transition, the emission frequency changes by the same amount so that the difference is kept the same.

source was a pulsed (50-ns width) CO_2 laser. The emission spectrum was measured using a Fourier transform interferometer. All lasing experiments were carried out with a sample temperature of 80 K. The lasing characteristics were well established in Refs. [8,9] where clear threshold and spectrometer-limited narrow line behaviors were shown.

For our structure, there are two materials components, GaAs and $\text{Al}_{0.35}\text{Ga}_{0.65}\text{As}$. There are therefore three LO-phonon modes: GaAs, GaAs-like, and AlAs-like, with the latter two associated with the $\text{Al}_{0.35}\text{Ga}_{0.65}\text{As}$ alloy. The characteristics of AlGaAs LO phonons are well studied and documented [16,17]. Taking the empirical expression [17] and the known temperature dependence [16], we obtain 293 (36.3), 280 (34.7), and 383 (47.5) cm^{-1} (meV) for the GaAs, GaAs-like, and AlAs-like modes, respectively, at 80 K. We have repeated some of the dielectric continuum model calculations in

Refs. [18,19]. We find that the GaAs, GaAs-like, and AlAs-like “interface” mode frequencies occur very close to their bulk values, practically independent of the changes of the structural parameters in the range used in the present work.

Our first Raman laser worked in near resonance with the AlAs-like phonon with an observed $\omega_{\text{pump}} - \omega_{\text{laser}} = 386 \text{ cm}^{-1}$ [9], close to the expected AlAs-like phonon value (383) but slightly larger. Since then, we have been investigating a wide range of parameters in the hope to observe Raman lasing with the GaAs phonon. At first sight, the GaAs phonon mediated process may be stronger than the AlAs-like phonon process, because the wave functions overlap the GaAs wells in the DQW. If, however, we adopt the results calculated using the dielectric continuum model [18,19], the interface phonons at both the GaAs and AlAs-like mode energies propagate through the DQW structure with nearly equal strengths and therefore cause 2-to-1 transitions with equal strengths. Our DQW wafers were designed to cover a range of 1-to-2 energy separations and yet to have the 1-to-3 transition falling into the CO_2 laser tuning range. For the required systematic change, we fix the barriers and vary only the well thicknesses. For the range of well thicknesses used, our samples give a range of 1-to-2 level separation of 28–42 meV which cover the GaAs phonon energy of about 36 meV.

For all samples, emission spectra were collected for different pumping wave numbers (frequencies). The spectra were taken with a spectrometer resolution of 1 cm^{-1} and the lasing peak positions were determined with an accuracy better than 1 cm^{-1} ($\sim 0.1 \text{ meV}$). Figure 2 shows the emission spectral peak position vs pump position (for about half of the samples to avoid overcrowding), with lasing wavelengths (wave numbers) from 12.0 (830) to 16.4 μm (610 cm^{-1}). Each type of symbol represents one sample. The gaps with no data in regions of 960, 985 to 1030, and 1060 cm^{-1} are due to the CO_2 laser tuning gaps. The inset to the figure shows the transmission spectrum for one sample at room temperature under a multipass 45° geometry. The data in Fig. 2 show that for a given sample the lasing peak shifts very uniformly to higher frequencies as the pump frequency is increased, with a unity slope—a characteristic of the Raman process. This means that for a given sample, the difference between the pump and emission frequencies is constant. Figure 3 plots this constant value of the difference between the emission peak and pumping positions as a function of the 1-to-2 level separation for all samples. Note that the difference plotted here is the Raman shift of the Stokes process. The x axis of Fig. 3 is based both on the absorption experiment (see the inset to Fig. 2 for one sample) and the calculation, with an error bar of about 1 meV. They are mutually consistent; i.e., the calculated separation corresponds to the difference between the 1-to-3 and 2-to-3 absorption positions, taking into

Our first joint publication

APPLIED PHYSICS LETTERS 87, 141102 (2005)

Effect of doping concentration on the performance of terahertz quantum-cascade lasers

H. C. Liu,^{a)} M. Wächter, D. Ban, Z. R. Wasilewski, M. Buchanan, and G. C. Aers
Institute for Microstructural Sciences, National Research Council, Ottawa KIA 0R6, Canada

J. C. Cao and S. L. Feng
State Key Laboratory of Functional Materials for Informatics, Shanghai Institute of Microsystem and Information Technology, Chinese Academy of Sciences, Shanghai 200050, China

B. S. Williams and Q. Hu
Department of Electrical Engineering and Computer Science and Research Laboratory of Electronics, Massachusetts Institute of Technology, Cambridge, Massachusetts 02139

(Received 8 February 2005; accepted 8 August 2005; published online 26 September 2005)

We characterized a set of terahertz quantum-cascade lasers with identical device parameters except for the doping concentration. The δ -doping density was varied from 3.2×10^{10} to $4.8 \times 10^{10} \text{ cm}^{-2}$. We observed that the threshold current density increased monotonically with doping. Moreover, the measured results on devices with different cavity lengths provided evidence that the free carrier absorption caused waveguide loss also increased monotonically. Interestingly, however, the observed maximum lasing temperature displayed an optimum at a doping density of $3.6 \times 10^{10} \text{ cm}^{-2}$. © 2005 American Institute of Physics. [DOI: 10.1063/1.2067699]

Since Köhler *et al.* reported a quantum-cascade laser (QCL) operating in the terahertz (THz) frequency range at 4.4 THz,¹ significant progress has been made over the past three years.^{2,3} For example, THz QCLs have been improved from lasing only at very low temperatures^{1,2} to 164 K (Ref. 4) and from operating only in pulsed mode¹⁻³ to continuous wave.⁵⁻⁷ Based on our current understanding, while we are able to choose the values of most device parameters, we are not able to predict the optimal amount of doping for a given design. In this letter, we present a systematic study of the effect of doping on the performance of THz QCLs.

The active region of the QCL wafer, similar to Ref. 6, is based on a four-well module design in which the THz generating transition is from a pair of anticrossed double-well states, the longitudinal-optical (LO) phonon-mediated relaxation occurs in a wide and doped subsequent well, and the injection to the following double well is from an undoped well. A schematic of the conduction-band profile is shown on the left part of Fig. 1, together with the calculated squared wave functions of the most important states. In order to isolate the effects solely due to doping, it is crucial to keep all the other parameters, including Al fraction and layer (well and barrier) thicknesses, unchanged while varying the doping concentration. This would be difficult to ensure by growing different wafers, due to the fluctuations in Ga and Al fluxes during the 20 h growth time for the present QCL design. To eliminate such uncertainty, a special molecular-beam epitaxy (MBE) growth procedure was employed. We used δ -doping with Si at the center of the 153-Å-thick "phonon" well and stopped the wafer rotation only during the doping, each time precisely aligning the wafer's [011] crystallographic direction along the Si cell azimuthal orientation (see Fig. 1). This resulted in a nearly linear gradient of the doping concentration across the 3 in. wafer which had otherwise identical layer thicknesses and aluminum fraction.

X-ray measurements indicated that the uniformity of layer thicknesses across the wafers was within $\pm 0.5\%$, while the Al fraction uniformity was better than ± 0.0003 . The wafer was grown on a semi-insulating GaAs substrate with 176 cascaded four-well modules made of GaAs wells and $\text{Al}_{0.15}\text{Ga}_{0.85}\text{As}$ barriers. Cladding and contact layers were the same as those in Ref. 6, except that the etch-stop layer was 0.1- μm -thick AlAs and the lower contact layer was 0.1- μm -thick n^+ GaAs, doped with Si to $5.0 \times 10^{18} \text{ cm}^{-3}$. Beginning with the injection barrier, the layer thicknesses of the four-well module are **54/78/24/64/38/153/35/88 Å**; where the barrier layers are shown in bold and the doped layer is underlined. A schematic of the wafer and the positions of the measured samples are shown on the right part of Fig. 1.

Four pieces (labeled A–D) were used for this study. By secondary ion mass spectroscopy (SIMS) measurements, their δ -doping densities were determined to be $3.2 \times 10^{10} \text{ cm}^{-2}$ (Sample A), $3.6 \times 10^{10} \text{ cm}^{-2}$ (B), $4.2 \times 10^{10} \text{ cm}^{-2}$ (C), and $4.8 \times 10^{10} \text{ cm}^{-2}$ (D), respectively. The

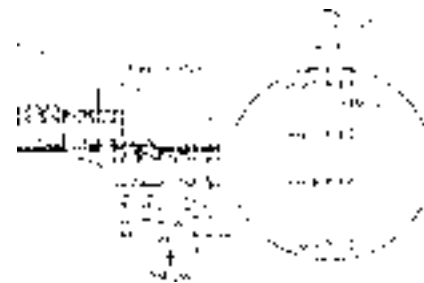


FIG. 1. Schematic conduction band profile, calculated wave functions, and schematic wafer layout.

^{a)}Electronic mail: h.c.liu@nrc.ca

Our most recent paper

Terahertz quantum cascade lasers operating up to ~ 200 K with optimized oscillator strength and improved injection tunneling

S. Fatholouloumi,^{1,3,*} E. Dupont,¹ C.W.I. Chan,² Z.R. Wasilewski,¹ S.R. Laframboise,¹ D. Ban,³ A. Mátyás,⁴ C. Jirauschek,⁴ Q. Hu,² and H. C. Liu^{1,5}

¹Institute for Microstructural Sciences, National Research Council, 1200 Montreal Rd, Ottawa, ON, K1A0R6, Canada

²Department of Electrical Engineering and Computer Science, Research Laboratory of Electronics, Massachusetts Institute of Technology, Cambridge, MA 02139, USA

³Department of Electrical and Computer Engineering, Waterloo Institute for Nanotechnology, University of Waterloo, 200 University Ave W., Waterloo, ON, N2L3G1, Canada

⁴Institute for Nanoelectronics, Technische Universität München, D-80333 München, Germany

⁵Currently with Key Laboratory of Artificial Structures and Quantum Control, Department of Physics, Shanghai Jiao Tong University, Shanghai 200240, China

*sfatholo@uwaterloo.ca

Abstract: A new temperature performance record of 199.5 K for terahertz quantum cascade lasers is achieved by optimizing the lasing transition oscillator strength of the resonant phonon based three-well design. The optimum oscillator strength of 0.58 was found to be larger than that of the previous record (0.41) by Kumar *et al.* [Appl. Phys. Lett. 94, 131105 (2009)]. The choice of tunneling barrier thicknesses was determined with a simplified density matrix model, which converged towards higher tunneling coupling strengths than previously explored and nearly perfect alignment of the states across the injection and extraction barriers at the design electric field. At 8 K, the device showed a threshold current density of 1 kA/cm², with a peak output power of ~ 38 mW, and lasing frequency blue-shifting from 2.6 THz to 2.85 THz with increasing bias. The wavelength blue-shifted to 3.22 THz closer to the maximum operating temperature of 199.5 K, which corresponds to $\sim 1.28\hbar\omega/k_B$. The voltage dependence of laser frequency is related to the Stark effect of two intersubband transitions and is compared with the simulated gain spectra obtained by a Monte Carlo approach.

© 2012 Optical Society of America

OCIS codes: (140.5965) Semiconductor lasers, quantum cascade; (40.5960) Semiconductor lasers.

References and links

1. R. Kohler, A. Tredicucci, F. Beltram, H. E. Beere, E. H. Linfield, A. G. Davies, D. Ritchie, R. C. Iotti, and F. Rossi, "Terahertz semiconductor-heterostructure laser," *Nature* **417**, 156–159 (2002).
2. B. S. Williams, S. Kumar, Q. Hu, and J. L. Reno, "Operation of terahertz quantum-cascade lasers at 164 K in pulsed mode and at 117 K in continuous-wave mode," *Opt. Express* **13**, 3331–3339 (2005).
3. H. Luo, S. R. Laframboise, Z. R. Wasilewski, and H. C. Liu, "Terahertz quantum cascade lasers based on a three-well active module," *Appl. Phys. Lett.* **90**, 041112 (2007).

#157687 - \$15.00 USD Received 21 Nov 2011; revised 17 Jan 2012; accepted 18 Jan 2012; published 1 Feb 2012
(C) 2012 OSA 13 February 2012 / Vol. 20, No. 4 / OPTICS EXPRESS 3866

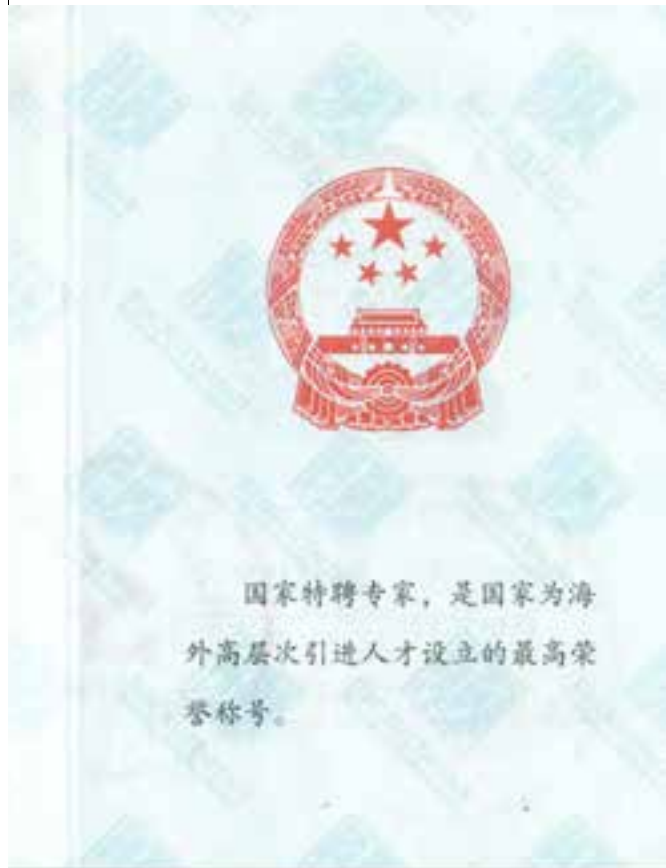
H. C. has established working relations in China more than 10 years ago



Went back to Shanghai for good in 2010



As part of the prestigious "1000-talent" program



中文姓名	刘惠春		
英文姓名	huichun liu		
国籍	加拿大		
身份证号		发证机关	中共中央组织部
护照号	BA177574		人力资源和社会保障部
出生年月	1963年03月	发证日期	2011年10月
		证书编号	0370

Was also a highly successful entrepreneur, started two companies



The company in Wuxi, focused on QWIPs.



A photo taken at 2011 ITQW, courtesy Emmanuel Dupont



H. C. will forever live in our memory

obituaries

To notify the community about a colleague's death, subscribers can visit <http://www.physicstoday.org/obituaries>, where they can submit obituaries (up to 750 words), comments, and reminiscences. Each month recently posted material will be summarized here, in print. Select online obituaries will later appear in print.

Hui-Chun Liu

Known for his groundbreaking work with semiconductor quantum devices, Hui-Chun Liu passed away on 23 October 2013 at age 53 in Shanghai, China; he had taken a bad fall and was in a coma the last nine days of his life. His sudden and unexpected death is a shock to the physics community.

Known to colleagues as H. C., he was born in Taiyuan, China, on 26 March 1960. He received his BSc in physics from Lanzhou University in 1982. After successfully passing the selection process for the second-year China-US Physics Examination and Application program, H. C. went to the University of Pittsburgh, where he received his PhD in applied physics in 1987 in the group of Darryl Coon. His major research interests were semiconductor nanoscience and quantum devices.

H. C. joined the Institute for Microstructural Sciences of the National Research Council Canada as a research associate in 1987 and rose rapidly through the ranks. In 1998 he was named to lead the council's terahertz and imaging devices group, and in 2000 he became a principal research officer—the highest rank, reserved for very few. In 2011 he returned to China to take a position at Shanghai Jiao Tong University, where as a chair professor he put together a new research group. H. C. had been recruited through the “1000 talents” program, which brings top minds to China from overseas. He founded two high-tech companies in China: Debut Optoelectronic Sensor in Wuxi and Ghopto Shanxi Guohui Optoelectronic Technology in Taiyuan.

Among H. C.'s honors were the Herzberg Medal from the Canadian Association of Physicists in 2000, the Bessel Prize from the Alexander von Humboldt Foundation in 2001, and the Jiangsu provincial high-level innovation-entrepreneur talent award in 2011. H. C. was granted more than a dozen patents, wrote or cowrote more than 380 articles in refereed journals, and gave 95 invited presentations at international conferences.

When H. C. was still in graduate school in the 1980s, the field of intersubband transitions in semiconductor



Hui-Chun Liu

quantum wells was born. H. C. was one of the founders of the field of quantum-well infrared photodetectors (QWIPs). As a junior researcher at National Research Council Canada, he started a world-leading research program on QWIPs. The ultrafast QWIP technologies he developed are being used in leading research laboratories and industries, including Harvard University, ETH Zürich, and Northrop Grumman. His patented upconversion pixel-less imagers have attracted considerable attention, as has his pioneering extension of QWIPs into the terahertz spectral region.

H. C.'s name has become synonymous with QWIP. He edited two volumes of the series Semiconductors and Semimetals and wrote a monograph on QWIPs. He served as chair or cochair of various QWIP workshops, was twice chair of the International Conference on Intersubband Transitions in Quantum Wells, and was a member of several steering and advisory committees overseeing the strategic development of terahertz technology in China.

In addition to his laying the foundations for the field of QWIPs, H. C. demonstrated two-photon absorption in QWIPs, studied various nonlinear optical phenomena through intersubband transitions, and developed an intersubband Raman laser. Early in his

career, he did innovative analysis on resonant tunneling diodes. More recently, he had focused on terahertz quantum cascade lasers and, with his collaborators, achieved a record-high operating temperature, which is significant, since increasing the lasers' operating temperature is the most important challenge in the field.

H. C. was like a brother to many of his colleagues around the world. A unique leader, he was generous with and fiercely protective of his staff, was attentive to their well-being, and knew instinctively how to draw out the best skills of each team member. He instilled a sense of common purpose in all. His calm and positive demeanor greatly influenced his colleagues and especially his students.

H. C.'s unfailing support and loyalty will be deeply missed, and he will always be fondly remembered.

We thank Chao Zhang (University of Wollongong) and Jun-Cheng Cao (Shanghai Institute of Microsystem and Information Technology) for their numerous contributions to this obituary.

Harald Schneider

Helmholtz-Zentrum Dresden-Rossendorf
Dresden, Germany

Qing Hu

Massachusetts Institute of Technology
Cambridge

Emmanuel Dupont

National Research Council Canada
Ottawa, Ontario

Xi-Cheng Zhang

University of Rochester
Rochester, New York

Kenneth Noble Stevens

On the day in 1954 when Kenneth Noble Stevens was first appointed at MIT as an assistant professor, no one could have predicted the number of scientific careers he would launch, the way he would transform the thinking of his students and colleagues, or the breadth of his influence on acoustic phonetics and beyond. He was a member of the MIT faculty for more than half a century and supervised at least 50 PhD students and an untold number of master's students, undergraduates, postdoctoral fellows, and visiting scientists. His first PhD student was James Flanagan in 1955, and his last one was Youngsook Jung in 2009.

Being in Ken's speech communication laboratory was an extraordinary experience. The lab was full of energy



THz QCL frequency combs, amplifiers, and antenna-coupled efficient emitters

Qing Hu (MIT)

September 9, 2014

David Burghoff, Tsung-Yu Kao, Ivan Chan, Xiaowei Cai, Yang Yang (MIT);
D. J. Hayton, J. N. Hovenier, J.R. Gao (SRON / TU Delft);
John Reno (Sandia)

nature photonics

JUNE 2014 VOL 8 NO 6
www.nature.com/naturephotonics

Convenient frequency
combs in the terahertz



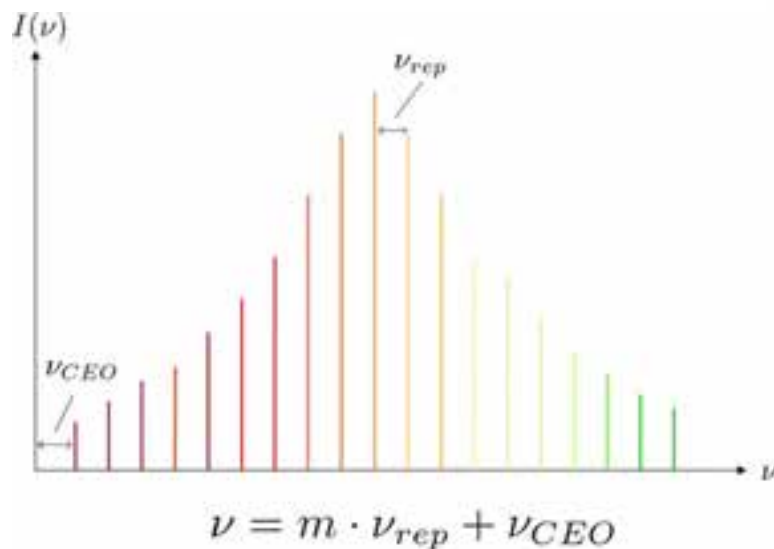
SOLAR CELLS
Lead-free perovskites

HIGH-ENERGY PHYSICS
Creating matter from light

BRAIN IMAGING
Optical tomography rises to the challenge

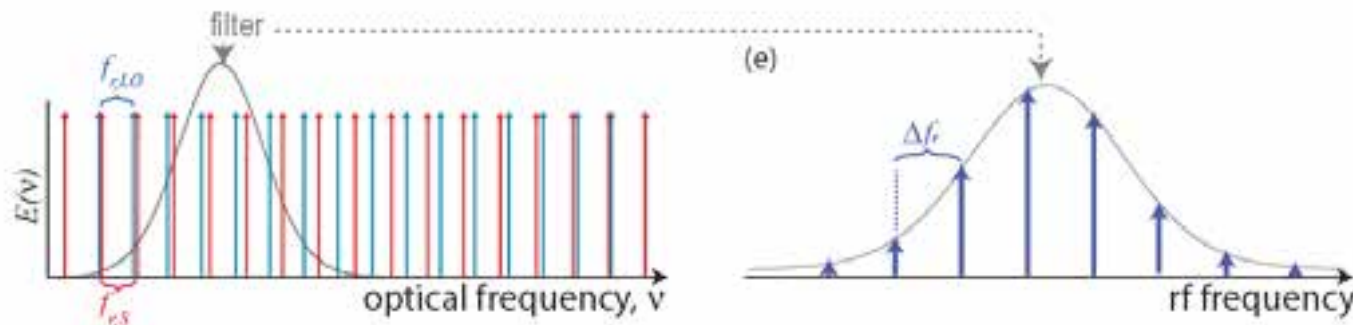
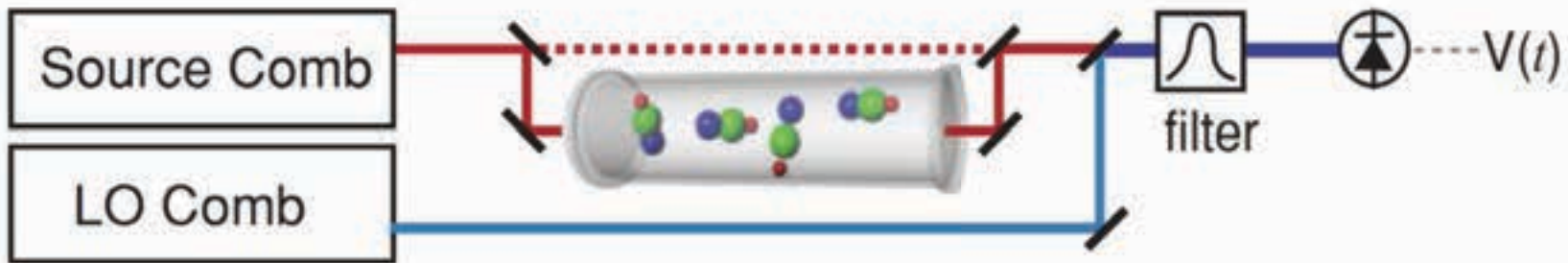
Frequency combs

- Light sources that consist of a large number of **evenly-spaced** laser lines
- Can be characterized by two parameters:
 - the spacing, f_{rep} (a.k.a. the repetition rate)
 - the offset frequency, f_{CEO} (a.k.a. the carrier-envelope offset)



Half of the 2005 Nobel Prize in Physics was awarded to John L. Hall and Theodor W. Hänsch "for their contributions to the development of laser-based precision spectroscopy, including the *optical frequency comb* technique".

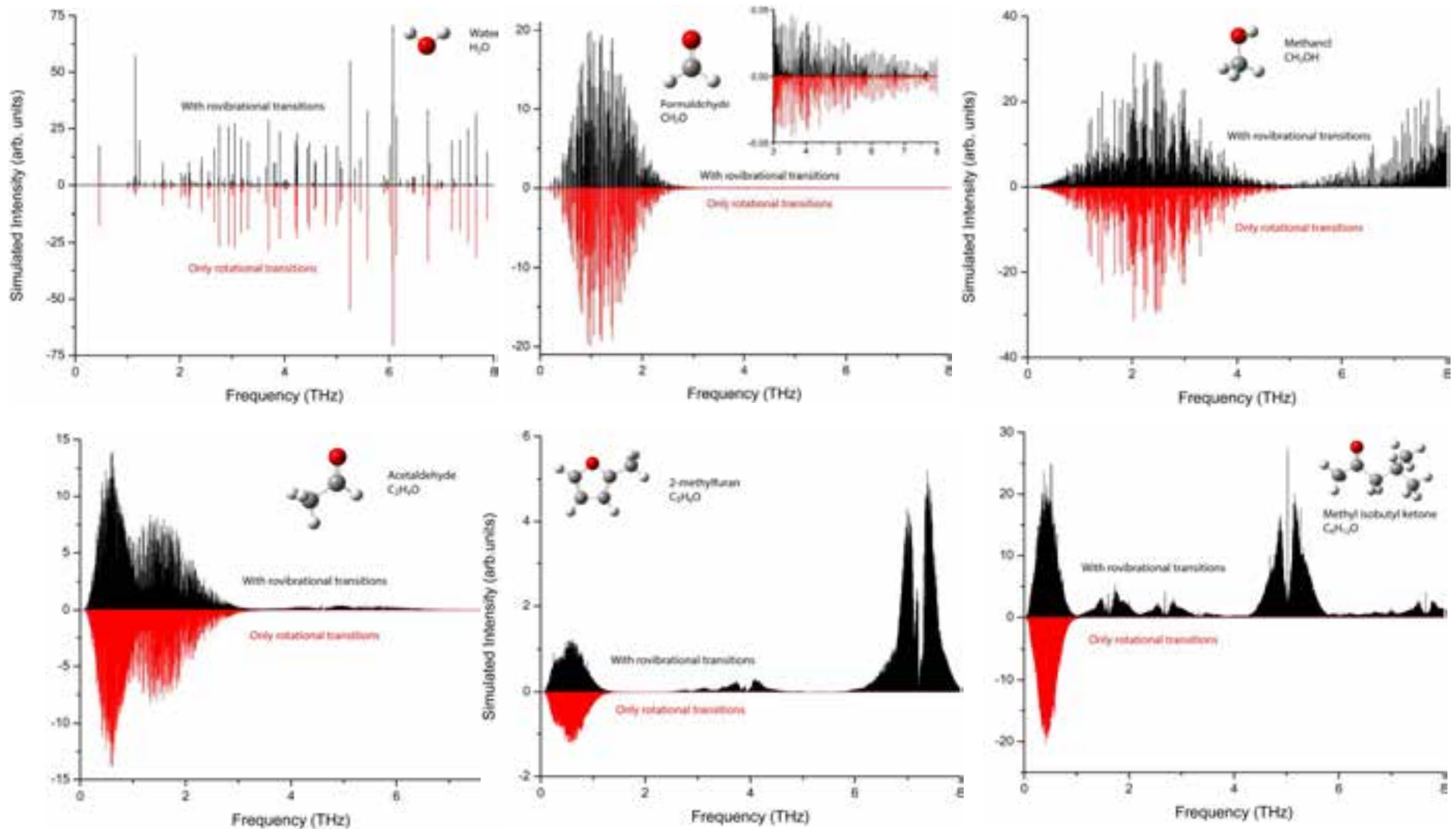
A very attractive method: dual-comb spectroscopy



(I. Coddington, *et. al*, *Physical Review A* **82**, 043817 (2010))

- Each rf component corresponds to the heterodyne beating between two comb lines
- By shining one through a sample, can get the sample's absorption profile
- Has the resolution and signal-to-noise of laser spectroscopy, the broadband capabilities of FTIR, and **no moving parts!**

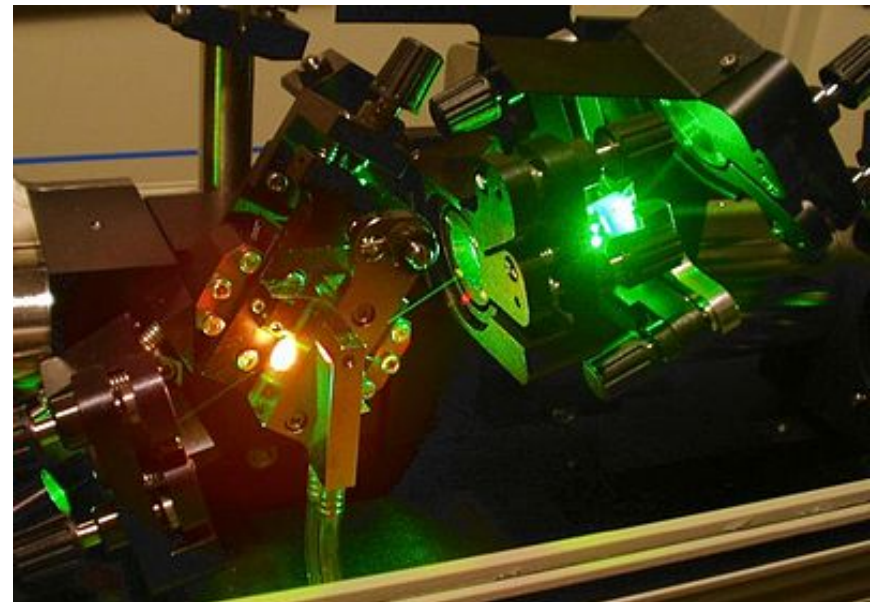
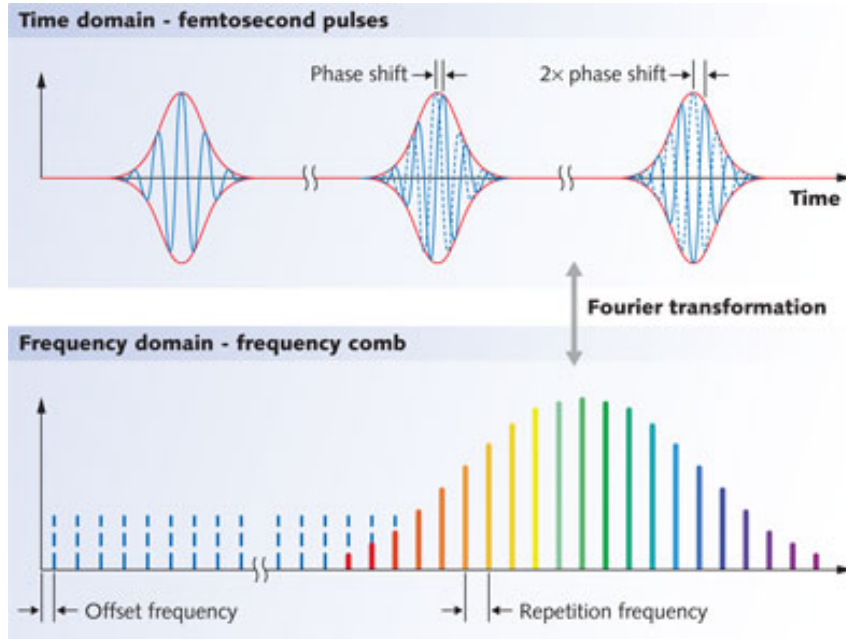
Examples of THz gas spectra



- Many gas molecules, especially as they get larger, have distinctive spectral lines at THz due to rovibrational transitions (results from Steve Shipman).

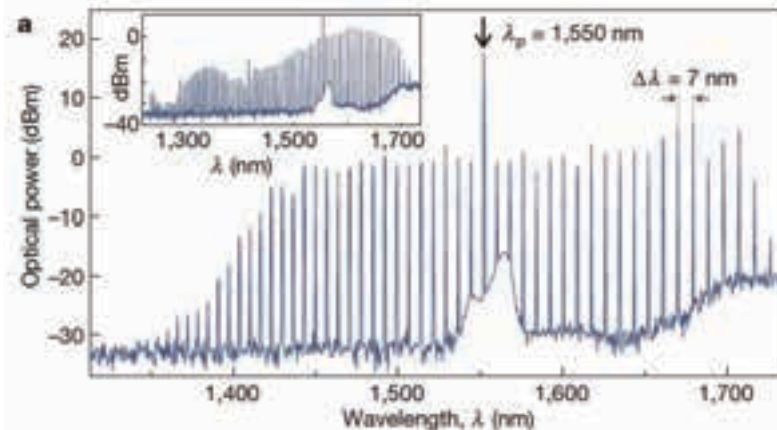
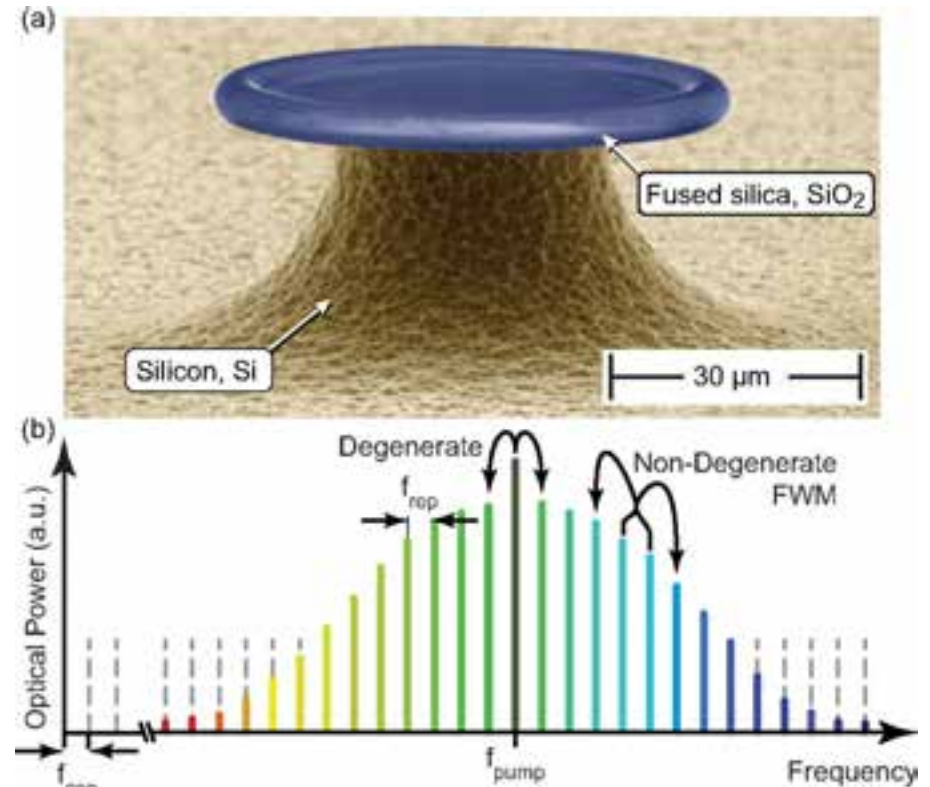
Types of frequency combs

- Historical work-horse: mode-locked lasers (e.g., Ti:Sapphire)
 - Pulse train in the time-domain, frequency comb in the frequency domain.
 - Extremely difficult to achieve in QCLs
 - gain recovers too quickly for stable pulses to form



Types of frequency combs (2)

- More recent development (2007): microresonator combs
 - Pump a high-Q resonator with narrow CW light, cascaded four-wave mixing ($\chi^{(3)}$) generates sidebands.
 - Cavity must have low dispersion, high Q.
 - Lines have a well-defined phase, but no pulses are formed.

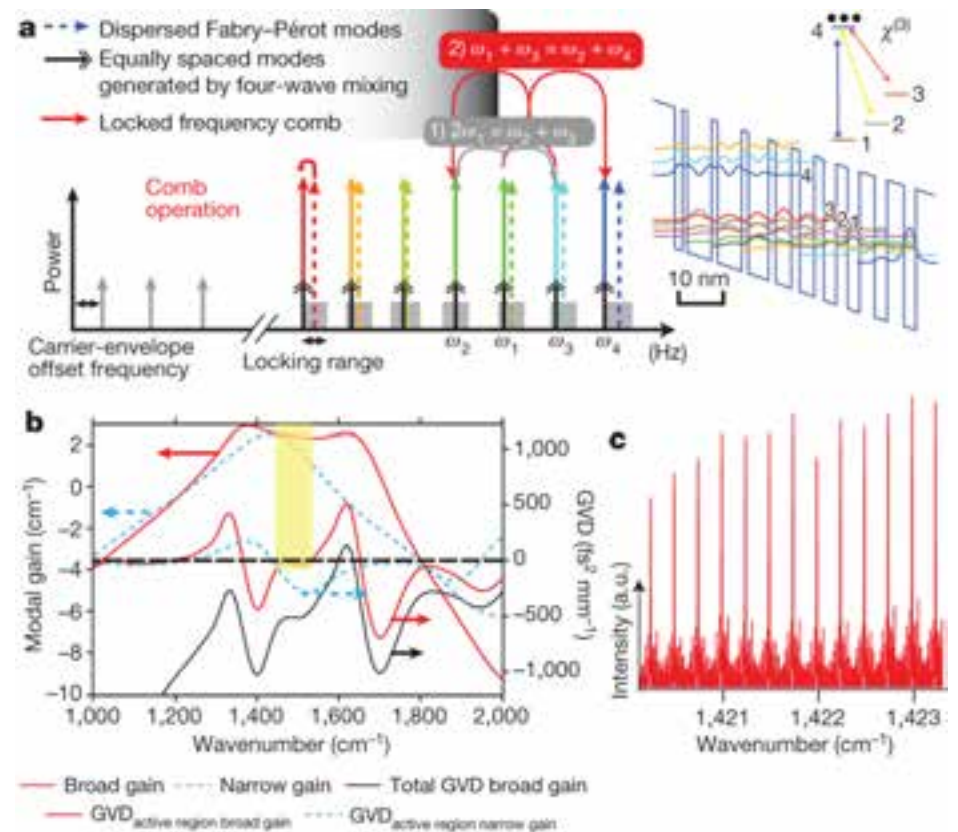


et al.

450

Types of frequency combs (3)

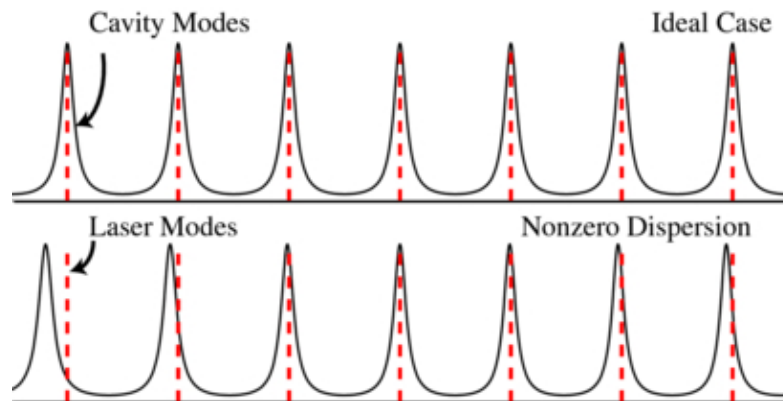
- More recent development (2012): microresonator-like combs in mid-IR QCLs
 - Low-dispersion, broadband gain media produces combs based on four-wave mixing
 - Cavity loss compensated by laser gain, high $\chi^{(3)}$ of gain medium
 - In the time-domain, the laser looks frequency-modulated at the repetition rate



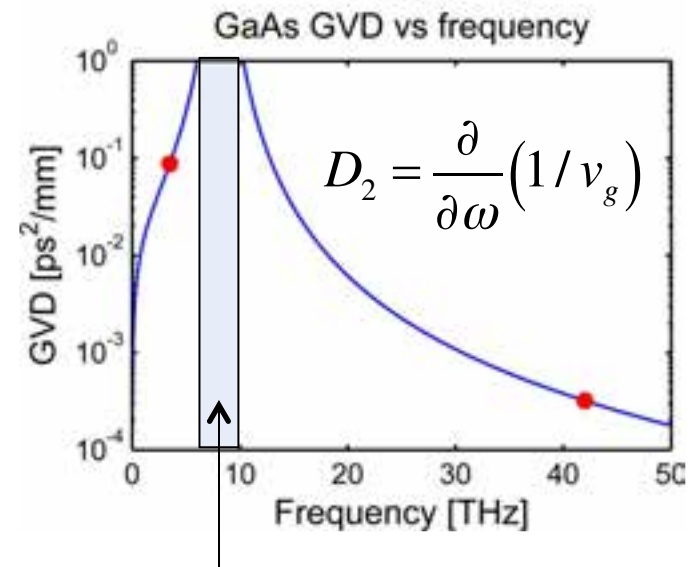
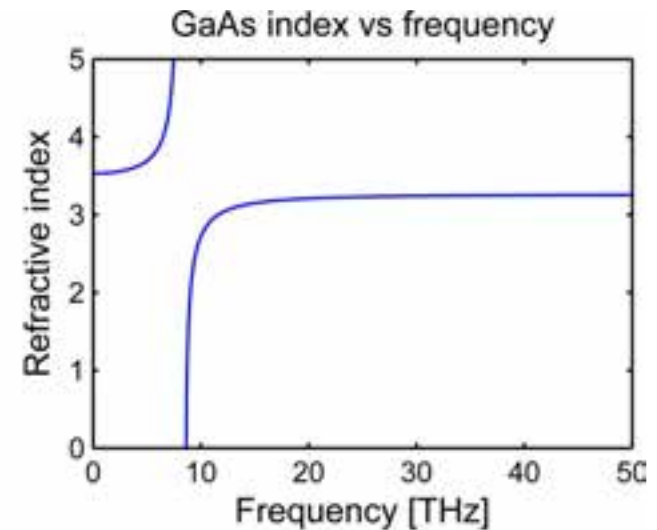
A. Hugi *et al.* Nature, **492**, 229 (2012)

Challenge at THz: Dispersion – the enemy of passive comb generation

- Group velocity dispersion (GVD) inhibits passive comb formation
 - Four-wave mixing combs: causes phase mismatch
 - Passively mode-locked lasers: causes pulse broadening
- III-V materials are particularly dispersive in THz
 - GaAs at 3.5 THz: 87,400 fs²/mm ~ **250 times of mid-IR GVD**
 - Frequencies separated by 1 THz will slip by $\lambda/4$ after only 130 μm !



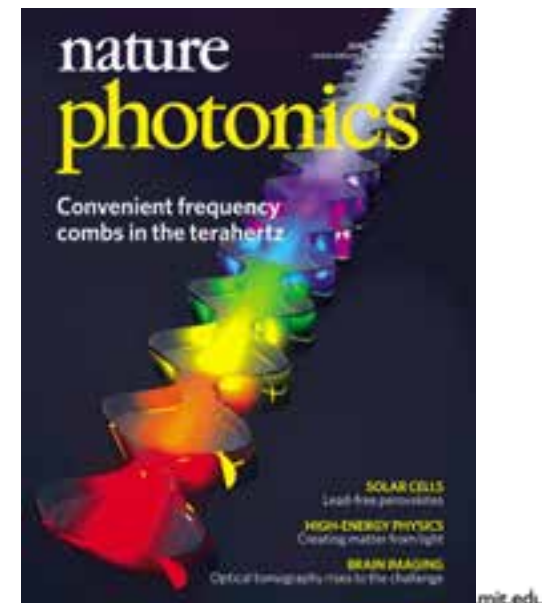
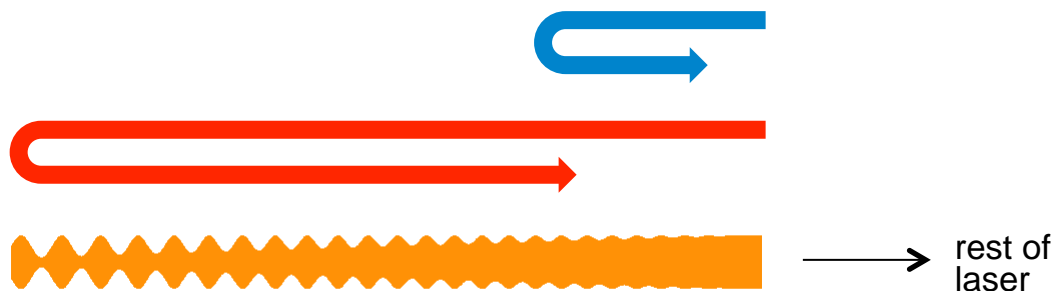
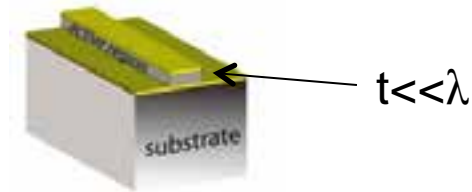
http://ej.iop.org/images/0953-4075/45/14/142001/Full/jpb410909f2_online.jpg



EM coupling to lattice (Reststrahlen band)

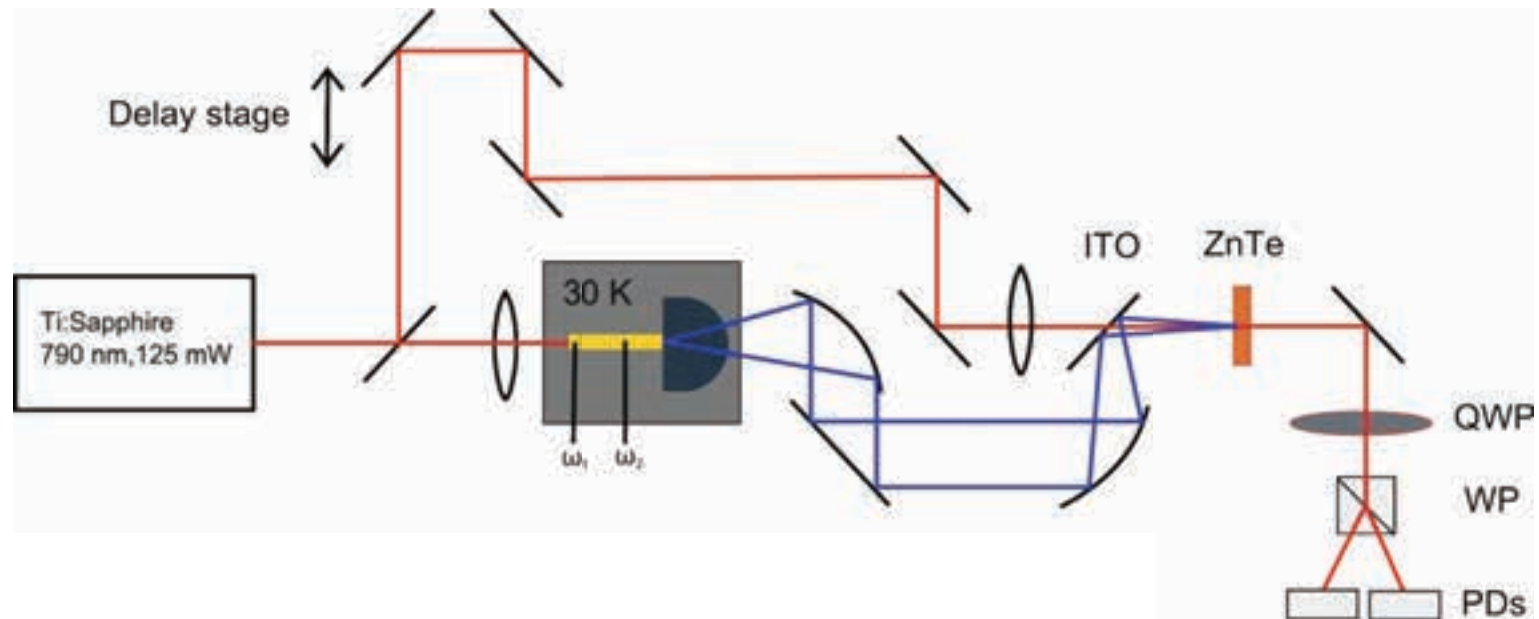
Dispersion compensation

- Many techniques have been developed for dispersion compensation in ultrafast lasers
 - grating pairs
 - prism pairs
 - double-chirped mirrors
- Name of the game is to counteract natural dispersion by delaying long wavelengths relative to short ones
- What techniques are accessible to THz QCLs based on metal-metal waveguides?



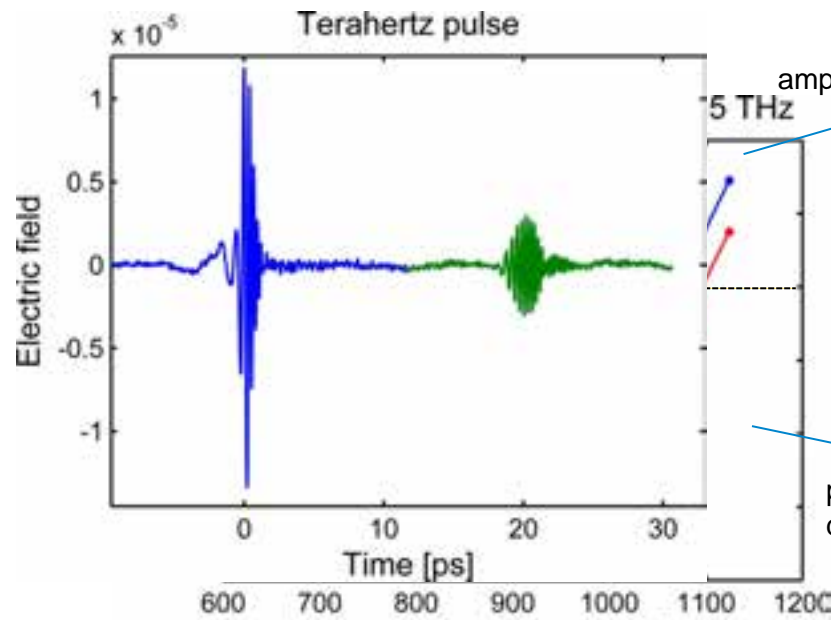
Actual cavity dispersion

- The previous calculation for GaAs ignored the gain medium and the waveguide. What's the real cavity dispersion?
 - Can be measured with terahertz time domain spectroscopy (THz-TDS)
 - QCL made to act like a photoconductive antenna
 - Like a sampling oscilloscope, you get the THz E-field vs time by repetitively sampling different time delays



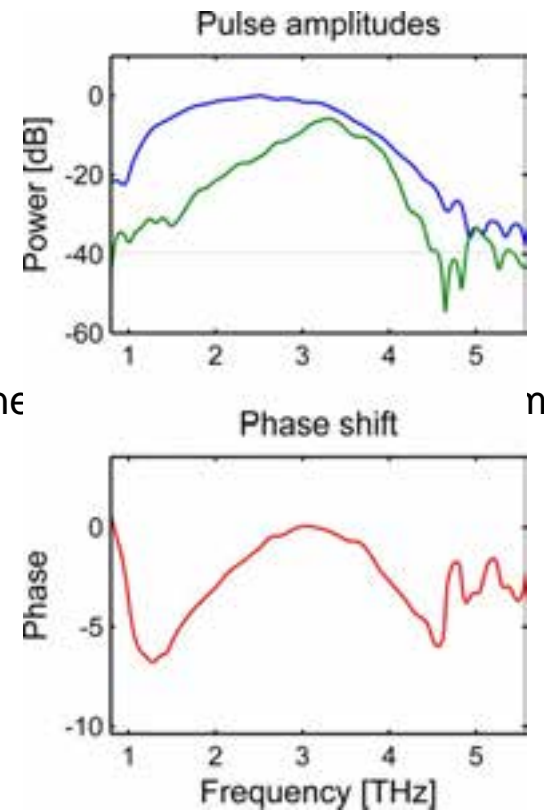
Actual cavity dispersion

- The previous calculation for GaAs ignored the gain medium and the waveguide. What's the real cavity dispersion?



Single-section laser, 774 μm long, 30 μm wide

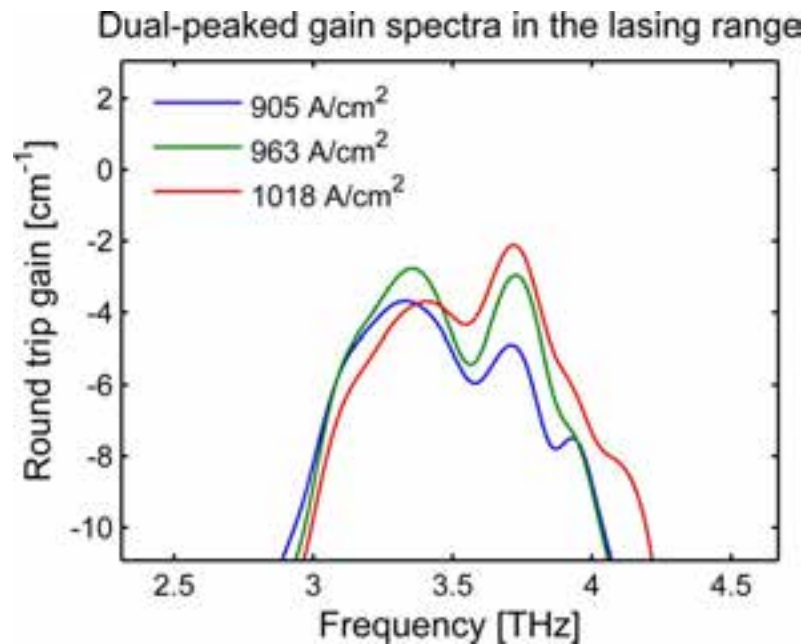
Design



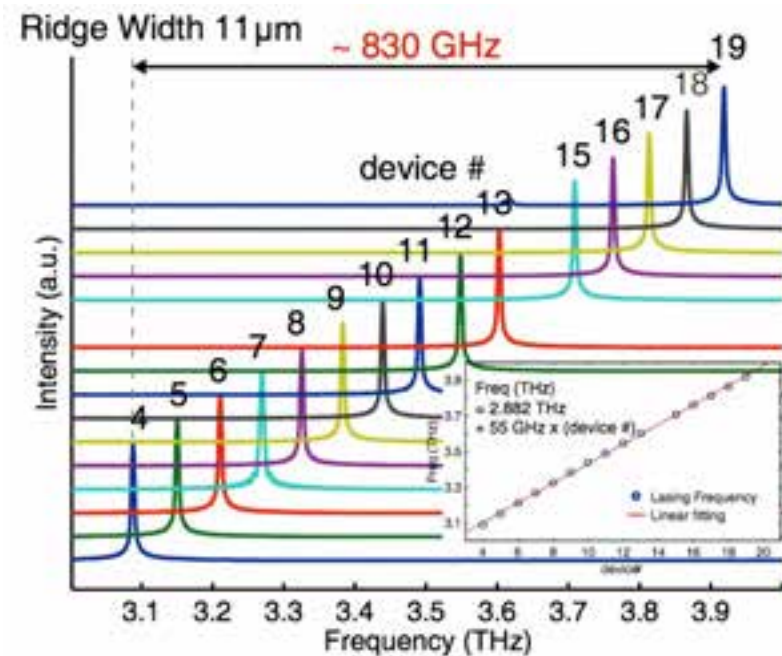
Nonlinear phase-frequency relation, highly dispersive

Gain medium

- Implemented on four-well resonant phonon gain medium with two-well injector ($T_{\max} \sim 170$ K)
- Gain medium is dual-peaked due to intra-injector splitting, has lobes at 3.3 THz and 3.8 THz
 - can lase over 800 GHz



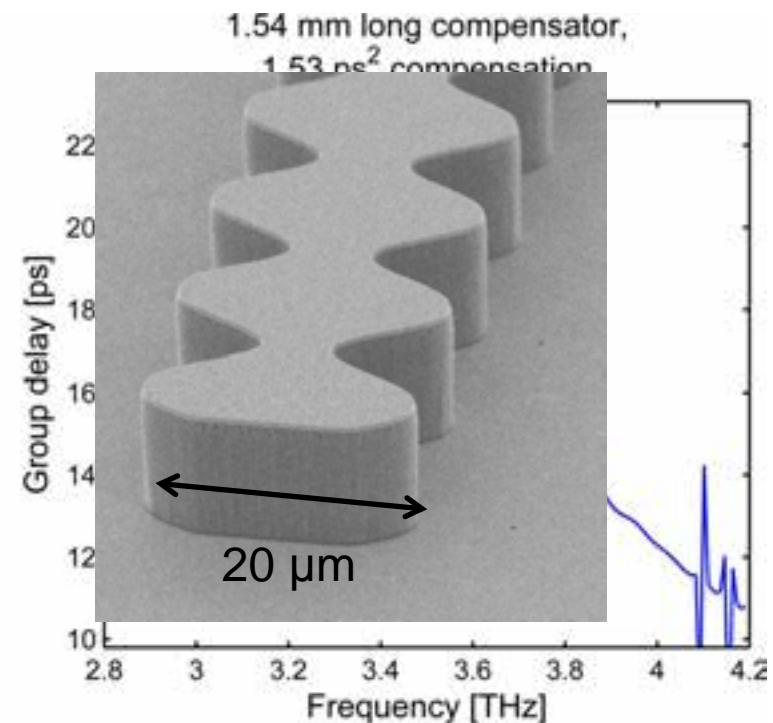
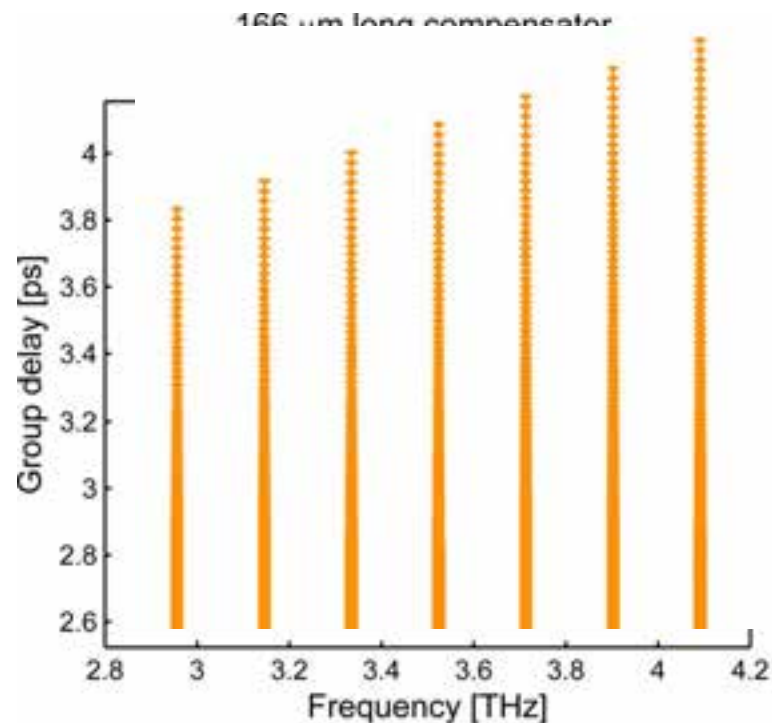
Single-section time domain measurement



Array of 3rd-order DFBs (not all the same bias)

Compensator designs

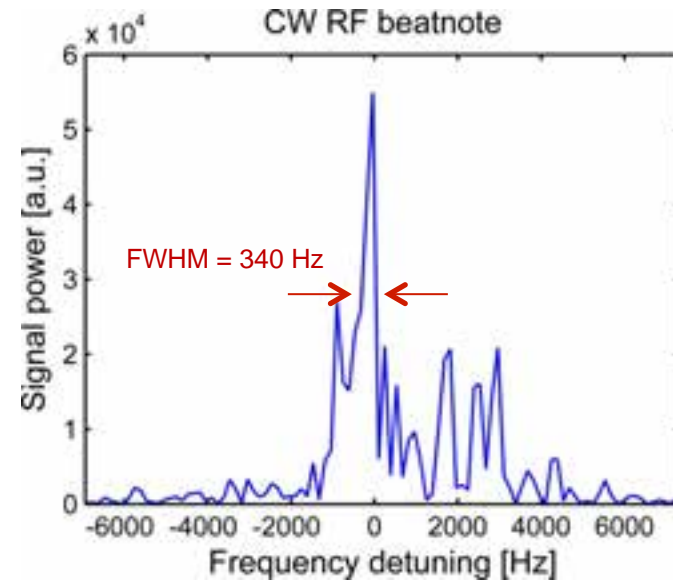
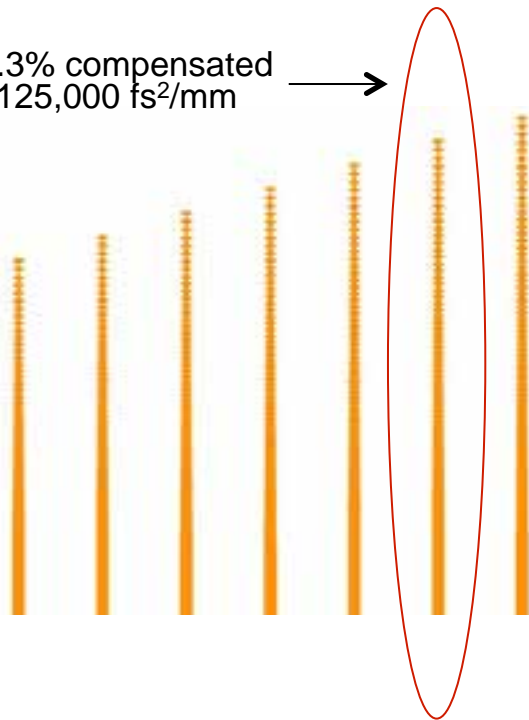
- FEM simulations used to determine group delay
- Sweep dispersion compensation to account for measurement uncertainty (0%, $\pm 6.6\%$, $\pm 13.3\%$, $\pm 20\%$)
- Compensation can be split over both facets or just one



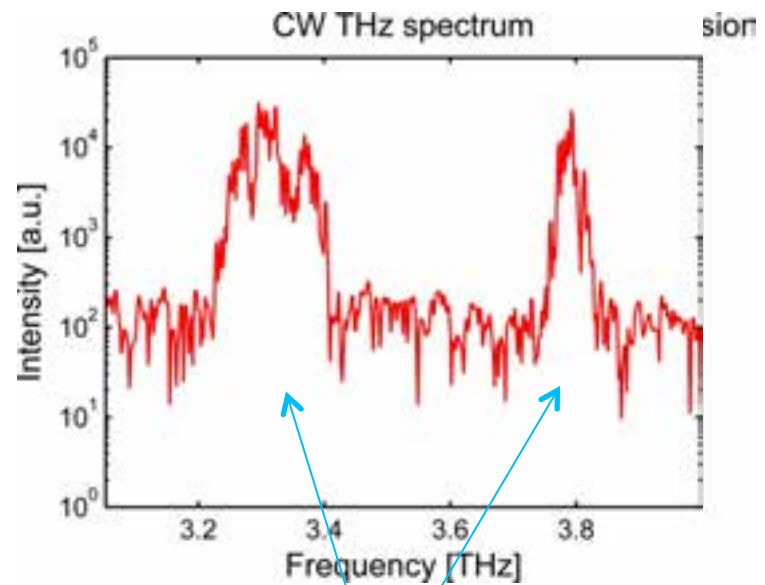
QCL bias tee beatnotes

- In each dispersion sweep series, only **one laser** (+13.3% overcompensated) produces broad spectra when DC-biased
- Same device produces strong narrowband RF signal at repetition rate (near 6.7 GHz, up to -14 dBm)

+13.3% compensated
 $D_2 = 125,000 \text{ fs}^2/\text{mm}$



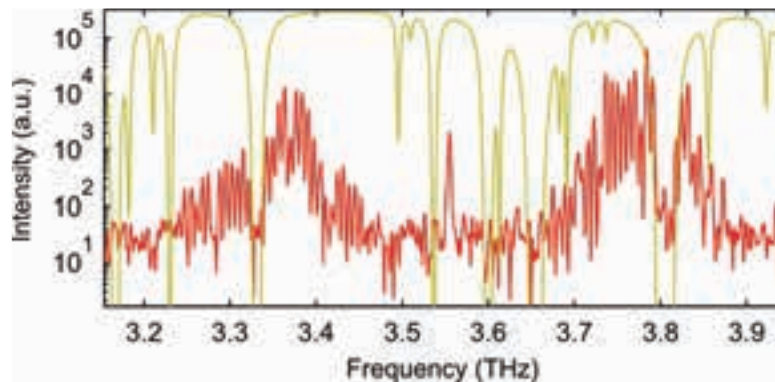
Compensated on both facets
 (feedback-insensitive)



from gain medium

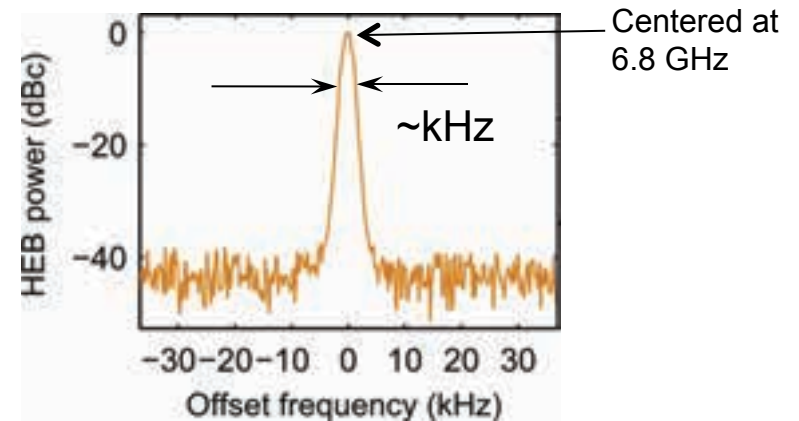
Key results #1: Spectrum and Beatnotes

1. Properly-compensated laser generates broadband spectrum when DC-biased (total power 5 mW at 45 K)

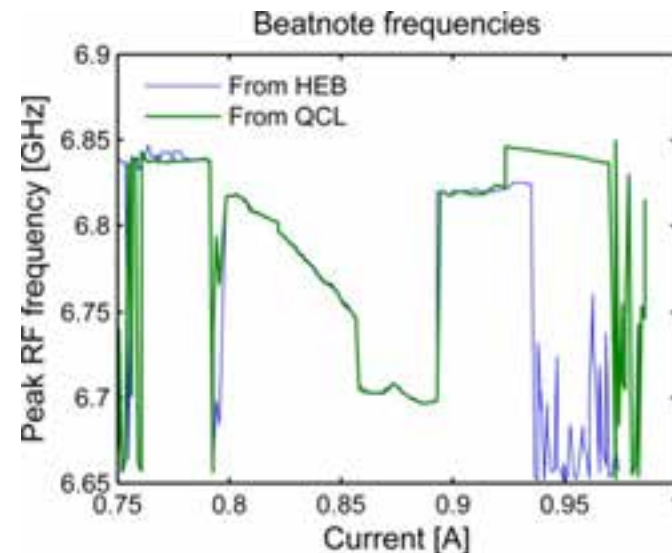


70 lines, 500 GHz total coverage
(14% of center frequency)

2. Laser produces narrow-linewidth beating on fast detector (hot electron bolometer or HEB)

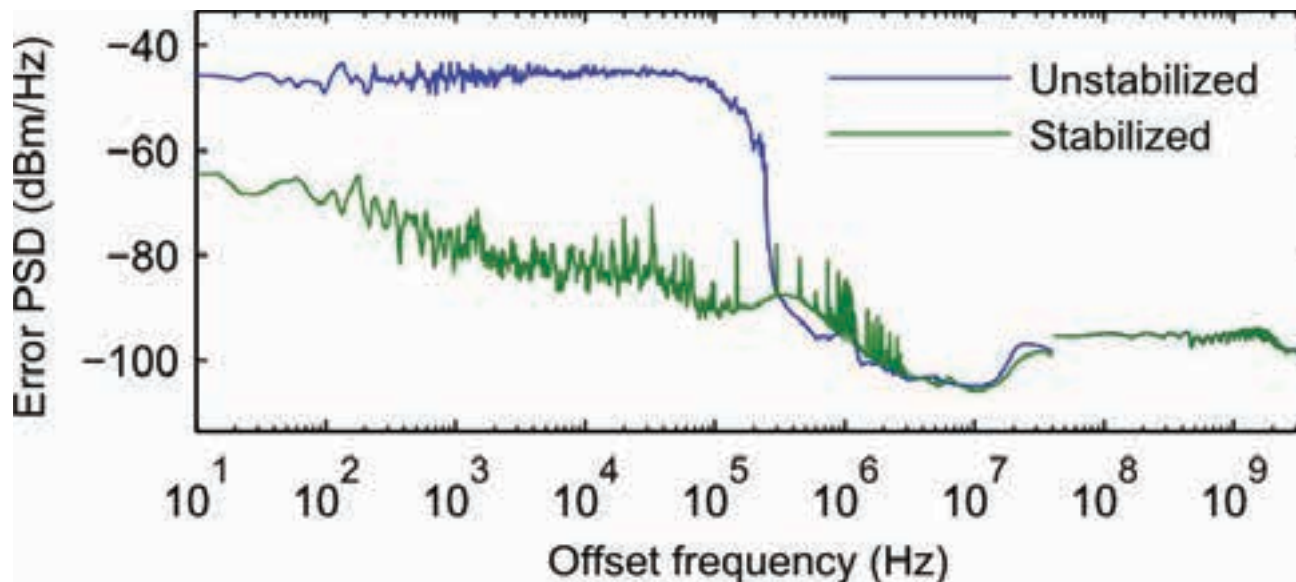


3. Beatnotes from QCL through bias-tee are similar to beatnotes observed from a remote fast detector (HEB).



Key results #2: narrow linewidth of the beatnote

- Beatnote can be stabilized to **sub-Hz** linewidths using PLLs with only <1 mA control current.



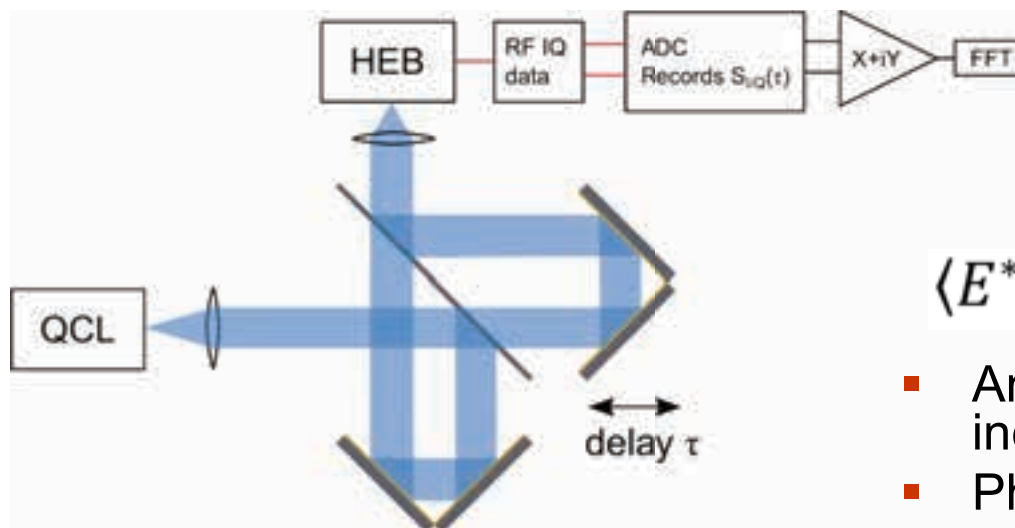
- The evidence is strong, but how can we be sure that we have a frequency comb?

Comb characterization

- A narrow beatnote can be generated by only a few (≥ 2) strong lines.
- Broad spectra can be just due to multi-mode lasing (eg. APL, **99**, 191104 (2011)).
- **SWIFT** (**S**hifted **W**ave **I**nterference **F**ourier **T**ransform) comes to the rescue.
- Not to be confused with a bird.

SWIFTS for Comb characterization

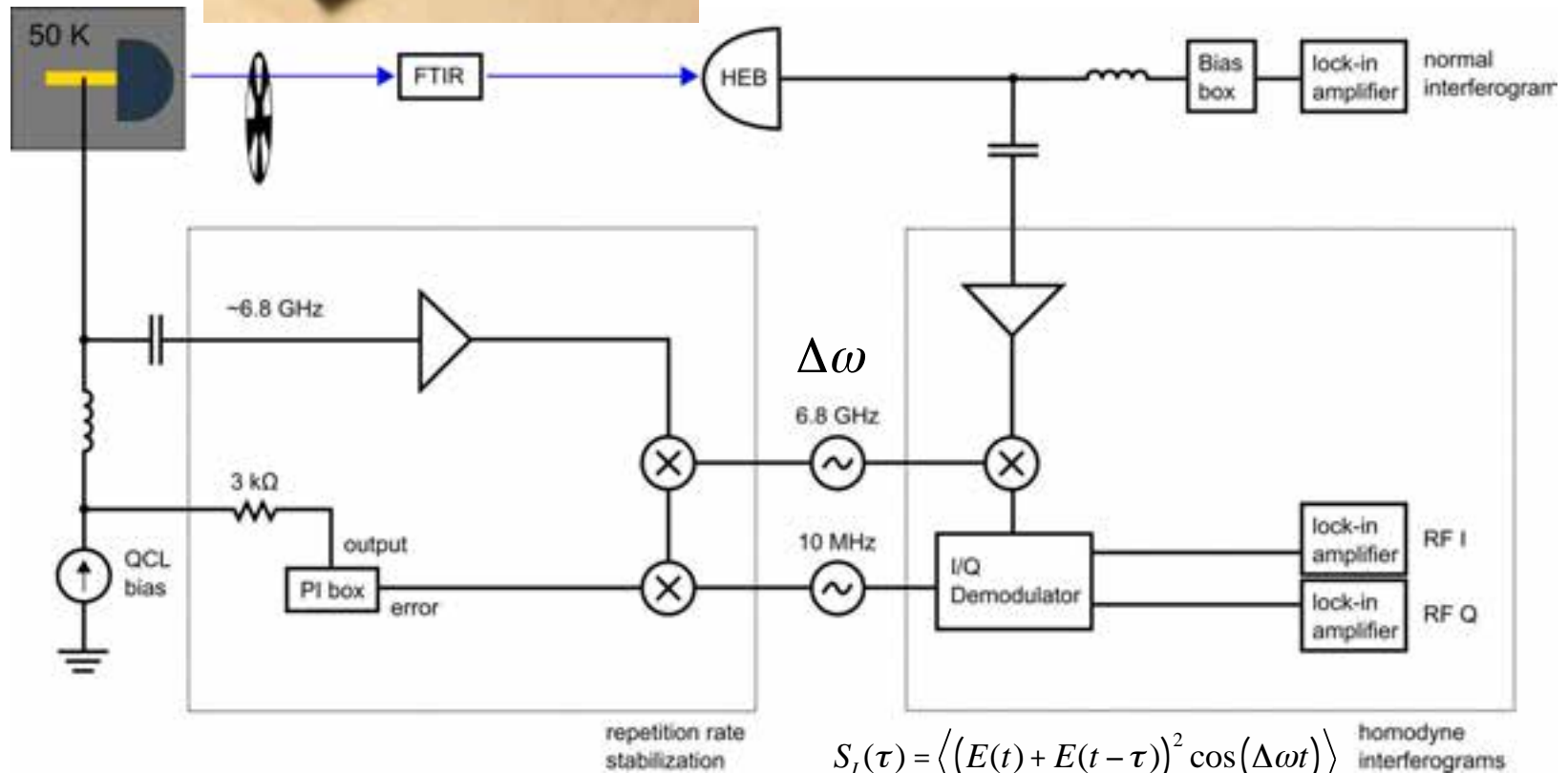
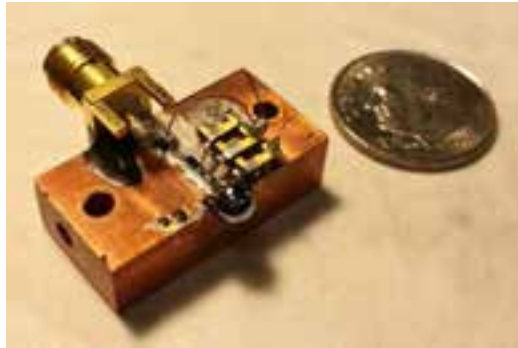
- **SWIFTS** (**S**hifted **W**ave **I**nterference **F**ourier **T**ransform **S**pectroscopy) is an extension of conventional FTS and **coherently** measures the beatnote.
- Measures RF quadratures of the beatnote as a function of delay in a Michelson spectrometer (the **fast-varying** part of the transmitted intensity).
 - It measures phase coherence among comb teeth at lab timescale of **~Hz**.
 - It measures the relative phase between two adjacent lines.



Measures
 $\langle E^*(\omega)E(\omega + \Delta\omega) \rangle$

- Amplitude vanishes if incoherent
- Phase is $\varphi(\omega + \Delta\omega) - \varphi(\omega)$

Detailed SWIFTS Setup



$$S_I(\tau) = \langle (E(t) + E(t - \tau))^2 \cos(\Delta\omega t) \rangle$$

$$S_Q(\tau) = \langle (E(t) + E(t - \tau))^2 \sin(\Delta\omega t) \rangle$$

First-principle derivation of conventional FTS and SWIFTS

For conventional FTS:

$$\begin{aligned}
 FTS &= \int_{\tau=-\infty}^{\infty} a(\tau) \langle E(t)E(t+\tau) \rangle_t e^{-j\omega\tau} d\tau \\
 &= A(\omega) * \mathcal{F} \left\{ \langle E(t)E(t+\tau) \rangle_t \right\}
 \end{aligned}$$

$a(\tau)$ – FTS apodization, $A(\omega) = \mathcal{F} \{ a(\tau) \} \sim$ GHz linewidth

$k(t)$ – lock-in window, $K(\omega) = \mathcal{F} \{ k(t) \} \sim$ Hz linewidth

$$\mathcal{F} \left\{ \langle E(t)E(t+\tau) \rangle_t \right\} = \int_{\tau=-\infty}^{\infty} \left[\int_{t=-\infty}^{\infty} k(t) \cdot E(t)E(t+\tau) dt \right] e^{-j\omega\tau} d\tau$$

switch the integration order of t and τ

$$\begin{aligned}
 &= \int_{t=-\infty}^{\infty} k(t) \cdot E(t) dt \left[\int_{\tau=-\infty}^{\infty} \underbrace{E(t+\tau)}_{\tau'} e^{-j\omega\tau} d\tau \right] \\
 &= \int_{t=-\infty}^{\infty} k(t) \cdot E(t) dt e^{j\omega t} \cdot E(\omega) \\
 &= [K(\omega) * E(\omega)]^* \cdot E(\omega)
 \end{aligned}$$

Thus, $FTS = A(\omega) * \left\{ [K(\omega) * E(\omega)]^* \cdot E(\omega) \right\} \approx A(\omega) * \left\{ E(\omega)^* \cdot E(\omega) \right\}$

First-principle derivation of conventional FTS and SWIFTS

For SWIFTS, it involves a time integration:

$$\langle E(t)E(t + \tau) \cos \Delta \omega t \rangle_t = \int_{t=-\infty}^{\infty} k(t) \cos \Delta \omega t \cdot E(t)E(t + \tau) dt$$

Clearly, only $E(\omega) \bullet E(\omega \pm \Delta \omega)$ contributes to this integration.

$$E(\omega)E(\omega \pm \Delta \omega) \propto \cos[\Delta \omega t + \phi(t)]$$

$\phi(t)$ – relative phase between $E(\omega)$ and $E(\omega \pm \Delta \omega)$

Thus

$$\int_{t=-\infty}^{\infty} k(t) \cos \Delta \omega t \cdot E(t)E(t + \tau) dt \propto \int_{t=-\infty}^{\infty} k(t) \cos[\phi(t)] dt$$

= 0 unless $\phi(t)$ is coherent within \sim Hz

SWIFTS interferograms will be **zero** for incoherent multi-mode lasing spectrum.

First-principle derivation of conventional FTS and SWIFTS

For non-zero SWIFTS:

The in – phase component

$$S_I(\omega) = \int_{\tau=-\infty}^{\infty} a(\tau) \langle E(t)E(t+\tau) \cos \Delta \omega t \rangle_t e^{-j\omega\tau} d\tau = A(\omega) * \mathcal{F} \left\{ \langle E(t)E(t+\tau) \cos \Delta \omega t \rangle_t \right\}$$

$$\mathcal{F} \left\{ \langle E(t)E(t+\tau) \cos \Delta \omega t \rangle_t \right\} = \int_{\tau=-\infty}^{\infty} \left[\int_{t=-\infty}^{\infty} k(t) \cos \Delta \omega t \cdot E(t)E(t+\tau) dt \right] e^{-j\omega\tau} d\tau$$

Again, switch the integration order of t and τ

$$= \int_{t=-\infty}^{\infty} k(t) \cos \Delta \omega t \cdot E(t) dt \left[\int_{\tau=-\infty}^{\infty} \underbrace{E(t+\tau)}_{\tau'} e^{-j\omega\tau} d\tau \right]$$

$$= \int_{t=-\infty}^{\infty} k(t) \cdot \cos \Delta \omega t \cdot E(t) dt e^{j\omega t} \cdot E(\omega)$$

$$= \left\{ \left[K(\omega) * \frac{1}{2} [E(\omega + \Delta \omega) + E(\omega - \Delta \omega)] \right] \right\}^* \cdot E(\omega)$$

Thus,
$$S_I(\omega) \approx A(\omega) * \left\{ \frac{1}{2} [E(\omega + \Delta \omega) + E(\omega - \Delta \omega)]^* \cdot E(\omega) \right\}$$

First-principle derivation of conventional FTS and SWIFTS

For SWIFTS:

$$\text{In-phase, } S_I(\omega) \approx A(\omega) * \left\{ \frac{1}{2} [E(\omega + \Delta\omega) + E(\omega - \Delta\omega)]^* \cdot E(\omega) \right\}$$

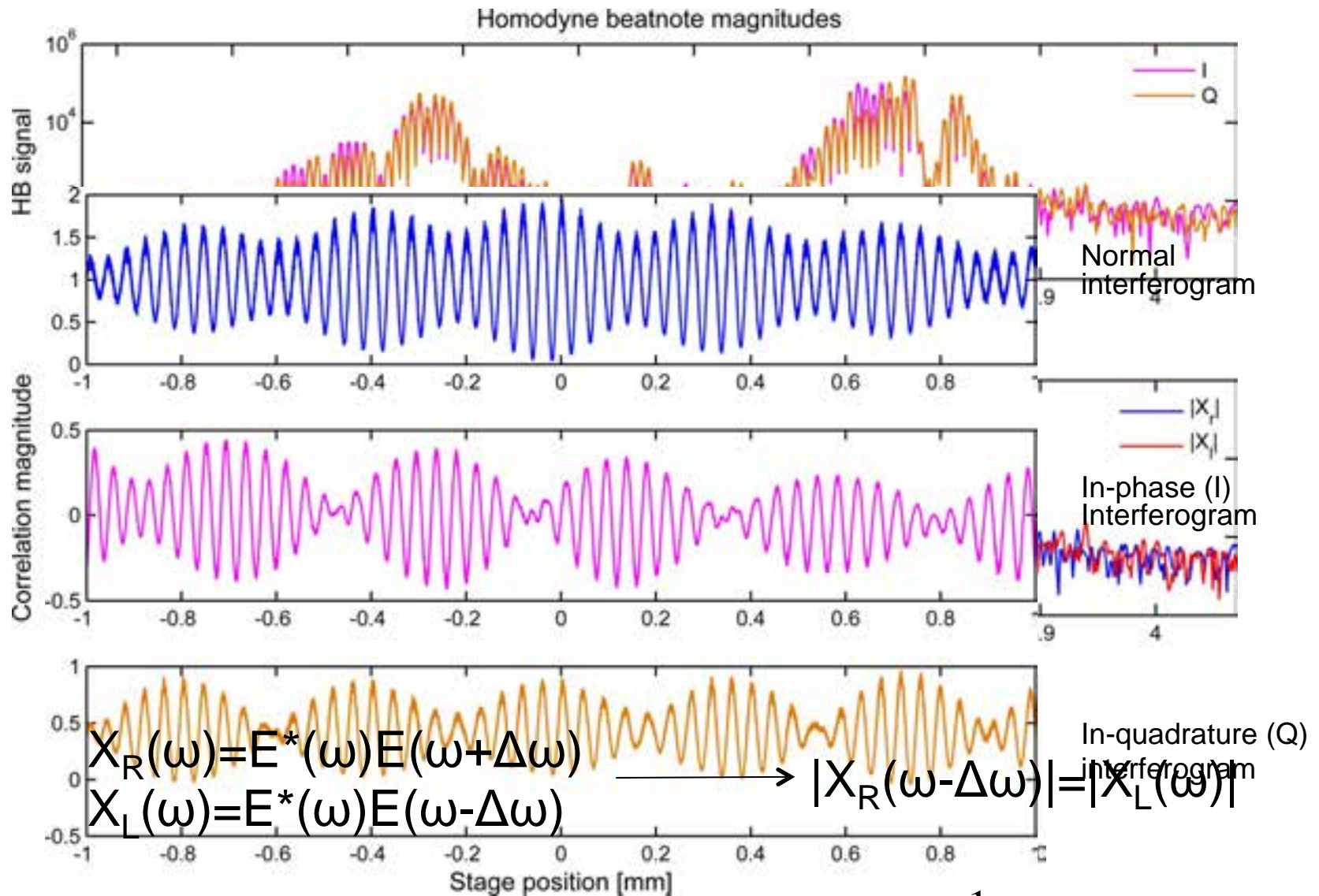
$$\text{similarly } S_Q(\omega) \approx A(\omega) * \left\{ \frac{1}{2j} [E(\omega - \Delta\omega) - E(\omega + \Delta\omega)]^* \cdot E(\omega) \right\}$$

$$\text{and } S_I(\omega) \pm jS_Q(\omega) \approx A(\omega) * \left\{ E(\omega \mp \Delta\omega)^* \cdot E(\omega) \right\}$$

It measures the relative phase of $E^*(\omega \mp \Delta\omega)E(\omega)$ accurate to the lock-in bandwidth of \sim Hz.

Note $E^*(\omega \mp \Delta\omega)E(\omega)$ is analogous to off diagonal elements in density matrix.

Homodyne beatnote interferometry (2)



$$X_{\pm}(\omega) = E^*(\omega)E(\omega \pm \Delta\omega) = \frac{1}{2} (S_I(\omega) \mp iS_Q(\omega)).$$

Key results #3: SWIFT results

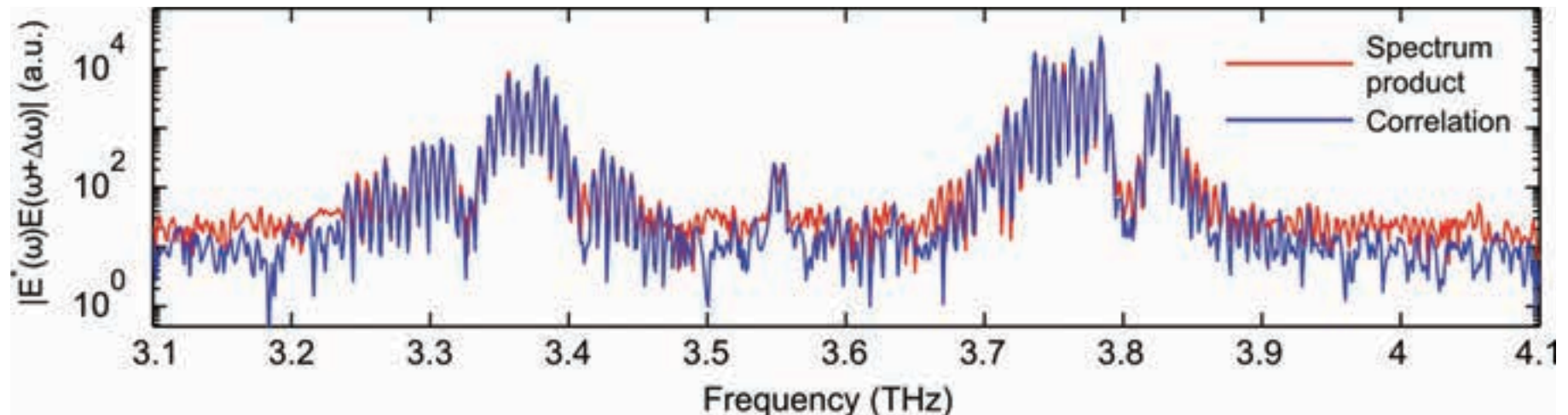
- SWIFT spectroscopy measures

$$X_{\pm}(\omega) = \langle E^*(\omega)E(\omega \pm \Delta\omega) \rangle \quad (\text{correlation})$$

while normal FTS can only be used to measure

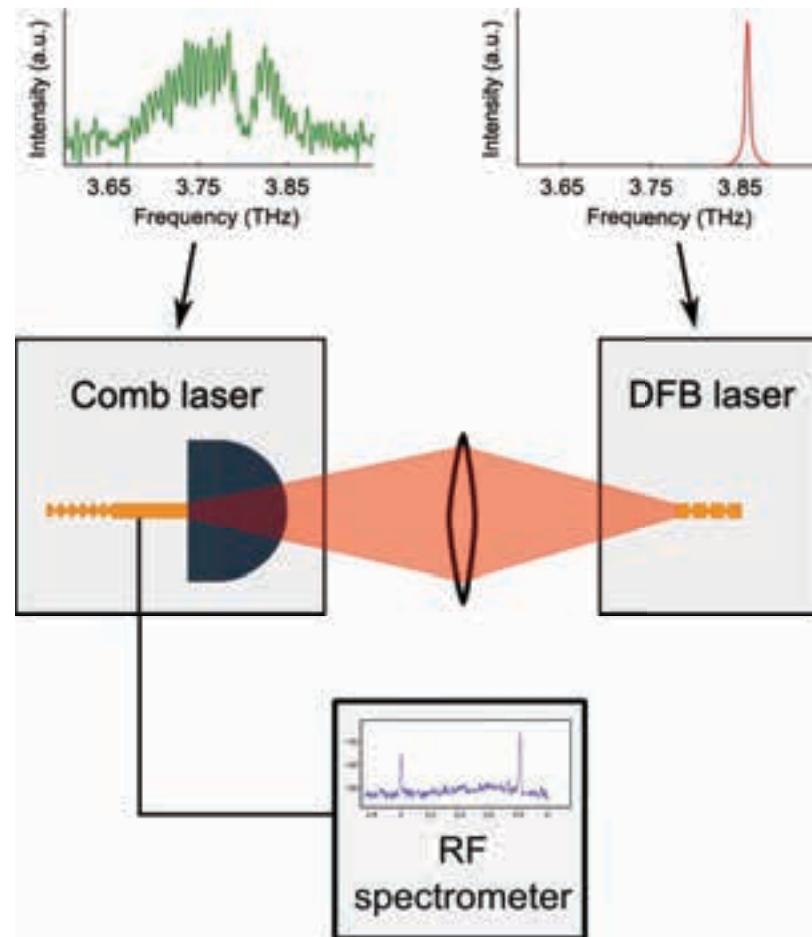
$$X_{\text{sp}}(\omega) = \sqrt{\langle |E(\omega)|^2 \rangle \langle |E(\omega + \Delta\omega)|^2 \rangle} \quad (\text{spectrum product})$$

- In general, $|X_{\text{sp}}(\omega)| \geq |X_{\pm}(\omega)|$. Equality can only be achieved when all of the modes are completely phase-coherent.



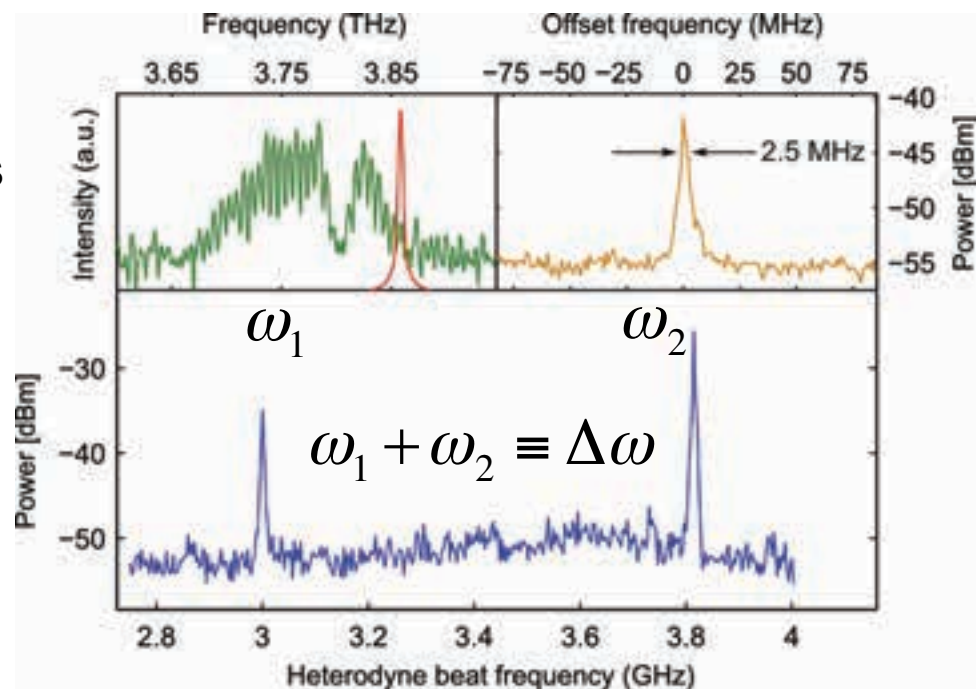
Key results #4: Absolute linewidth

- To probe absolute linewidth of comb lines, inject light from a narrowband (DFB) laser into comb cavity and measure intracavity beating between them



Key results #4: Absolute linewidth

- To probe absolute linewidth of comb lines, inject light from a narrowband (DFB) laser into comb cavity and measure intracavity beating between them
 - Two beatnotes observed that sum to the repetition rate
 - Measured linewidth is 2.5 MHz, deconvolved linewidth is 1.8 MHz (similar to free-running THz QCLs)
 - Good enough for dual comb spectroscopy, which would require ~ 10 MHz linewidth
- Comb is “measuring” the frequency of the DFB laser directly



Conclusions

- Demonstrated that by suitable dispersion engineering, THz QCLs can produce broadband frequency combs
 - 500 GHz total coverage, 70 lines, 5 mW
- Developed SWIFTS, an interferometric technique that can be used to measure phase coherence of a frequency comb
 - It can also be used as a pulse characterization technique since it measures phase, like FROG and SPIDER
- Showed that the absolute linewidth of each comb line is comparable to that of typical THz QCLs and is suitable for dual-comb spectroscopy
 - Possible to use intracavity mixing to make detector-free system?